Department of Chemistry

Characterization of nanostructured catalysts and silicon microstructures in polymer electrolyte membrane fuel cells

Petri Kanninen

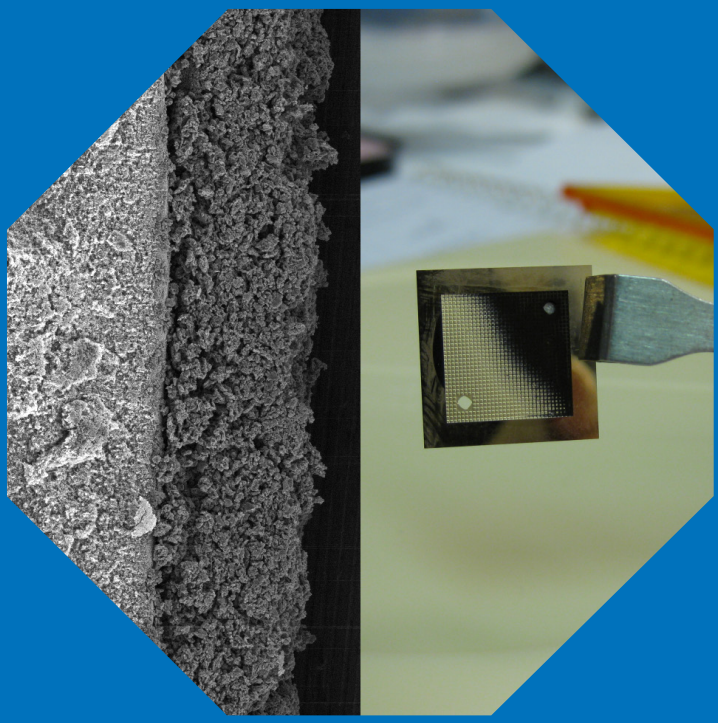

Aalto University

DOCTORAL DISSERTATIONS

Aalto University publication series
DOCTORAL DISSERTATIONS 76/2014

Characterization of nanostructured catalysts and silicon microstructures in polymer electrolyte membrane fuel cells

Petri Kanninen

Doctoral dissertation for the degree of Doctor of Science in Technology to be presented with due permission of the School of Chemical Technology for public examination and debate in Auditorium KE2 (Komppa Auditorium) at the Aalto University School of Chemical Technology (Espoo, Finland) on the 18th of June, 2014, at 12 noon.

Aalto University
School of Chemical Technology
Department of Chemistry
Research Group of Electrochemical Energy Conversion and Storage

Supervising professor
Professor Kyösti Kontturi

Thesis advisor
Dr. Tanja Kallio

Preliminary examiners
Dr. Frédéric Jaouen, Université Montpellier II, France
Professor Carita Kvarnström, University of Turku, Finland

Opponent
Professor Enn Lust, University of Tartu, Estonia

Aalto University publication series
DOCTORAL DISSERTATIONS 76/2014

ISBN 978-952-60-5702-6
ISBN 978-952-60-5703-3 (pdf)
ISSN-L 1799-4934
ISSN 1799-4934 (printed)
ISSN 1799-4942 (pdf)
http://urn.fi/URN:ISBN:978-952-60-5703-3

Unigrafia Oy
Helsinki 2014

Finland

441 697
Printed matter

Author
Petri Kanninen

Name of the doctoral dissertation
Characterization of nanostructured catalysts and silicon microstructures in polymer electrolyte membrane fuel cells

Publisher School of Chemical Technology

Unit Department of Chemistry

Series Aalto University publication series DOCTORAL DISSERTATIONS 76/2014

Field of research Physical Chemistry

Manuscript submitted 27 February 2014 **Date of the defence** 18 June 2014

Permission to publish granted (date) 13 May 2014 **Language** English

☐ **Monograph** ☒ **Article dissertation (summary + original articles)**

Abstract

Direct methanol fuel cells (DMFC) produce electrical energy directly from chemical energy. They are a promising candidate for power sources of portable devices due to the high energy density of methanol and the quick recharging procedure by fuel insertion. However, the problem areas of the DMFC are the slow electro-oxidation of methanol and the permeated methanol reacting at the cathode. New catalysts are constantly searched but they are often tested only for catalytic activity and the DMFC testing is omitted even though the catalyst layer (CL) structure has a large impact on the performance. Miniaturization of the system is also necessary for portable applications. Silicon etching can be used to fabricate small structures for fuel cells replacing or enhancing the functions of laboratory-scale components.

In the first part of this thesis, new catalysts for the DMFC are studied with the emphasis on the CL structure. Different carbon supports for the anode were studied: standard carbon black and alternative few-walled carbon nanotubes (FWCNT) and graphitized carbon nanofiber (GNF). The alternative supports showed better DMFC performance but their stability was lower than with carbon black. However, the CL formed with GNF showed a very porous structure enhancing the mass transfer, so that higher binder content could be used improving the stability to the level of carbon black and the performance by 30%. The FWCNTs were also investigated as a platform for enzymatic methanol oxidation by studying the electrochemical properties of an immobilized cofactor pyrroloquinoline quinone (PQQ). A large amount of PQQ was adsorbed having a strong redox response and good stability in a wide pH window. For the cathode, a methanol-tolerant, Pt-free nitrogen-doped FWCNTs were tested in an alkaline DMFC as such testing is not often made. Its performance was remarkably 4 times better than with Pt when synthetic air was used as the oxidant.

In the second part of thesis, an integrated gas diffusion layer (GDL) consisting of Si nanoneedles (nanograss) was tested in a micro fuel cell (MFC). The layer functioned properly at low current densities. For high power applications, a standard carbon cloth GDL was tested with the nanograss as a contact surface reducing the resistance between the GDL and the flow field. The use of the nanograss improved the MFC performance and stability. Finally, the MFCs were used as a catalyst testing platform and the results were compared with a similar test in a laboratory-scale DMFC. The results varied showing that the DMFC components also have a large impact on catalyst testing.

Keywords direct methanol fuel cell, carbon nanomaterials, micro fuel cells, catalyst layer

ISBN (printed) 978-952-60-5702-6 **ISBN (pdf)** 978-952-60-5703-3

ISSN-L 1799-4934 **ISSN (printed)** 1799-4934 **ISSN (pdf)** 1799-4942

Location of publisher Helsinki **Location of printing** Helsinki **Year** 2014

Pages 143 **urn** http://urn.fi/URN:ISBN:978-952-60-5703-3

Aalto-yliopisto

Tiivistelmä

Aalto-yliopisto, PL 11000, 00076 Aalto www.aalto.fi

Tekijä
Petri Kanninen

Väitöskirjan nimi
Nanorakenteisten katalyyttien ja piimikrorakenteiden tutkimus polymeerielektrolyyttimembraanipolttokennossa

Julkaisija Kemian tekniikan korkeakoulu

Yksikkö Kemian laitos

Sarja Aalto University publication series DOCTORAL DISSERTATIONS 76/2014

Tutkimusala Fysikaalinen kemia

Käsikirjoituksen pvm 27.02.2014 **Väitöspäivä** 18.06.2014

Julkaisuluvan myöntämispäivä 13.05.2014 **Kieli** Englanti

☐ **Monografia** ☒ **Yhdistelmäväitöskirja (yhteenveto-osa + erillisartikkelit)**

Tiivistelmä

Suorametanolipolttokennot (SMPK) tuottavat sähköenergiaa suoraan kemiallisesta energiasta. Ne ovat lupaava vaihtoehto kannettavien laitteiden voimanlähteeksi, koska metanolilla on korkea energiatiheys ja lataaminen tapahtuu nopeasti polttoainelisäyksellä. SMPK:lla on kuitenkin rajoitteina metanolin hidas hapetusreaktio ja katodille kulkeutuneen metanolin reagoiminen. Uusia katalyyttejä etsitään jatkuvasti, mutta ne testataan usein vain aktiivisuuden osalta ja SMPK-testaus jätetään pois, vaikka katalyyttikerroksen (KK) rakenne vaikuttaa huomattavasti SMPK:n toimintaan. Systeemin pienentäminen on myös tärkeää kannettavia sovelluksia varten. Piin etsaaminen on tapa tuottaa pieniä rakenteita polttokennoihin korvaamaan ja tehostamaan perinteisten komponenttien toimintaa.

Väitöskirjan 1. osassa tutkittiin uusia katalyyttejä SMPK:ta varten painottaen KK:n rakennetta. Anodilla tarkasteltiin tukiaineiden vaikutusta perinteisen hiilimustan ja vaihtoehtoisten hiilinanoputkien ja hiilinanokuitujen kanssa. Vaihtoehtoiset aineet olivat tehokkaampia SMPK:ssa, mutta niiden stabiilius ei ollut hiilimustan tasolla. Hiilinanokuidut kuitenkin muodostivat hyvin huokoisen KK:n parantaen aineensiirtoa, joten sidosaineen määrä voitiin nostaa niin, että stabiilius nousi hiilimustan tasolle ja suorituskyky 30 %. Hiilinanoputkia tutkittiin myös entsymaattisessa metanolin hapetuksessa immobilisoimalla sen pinnalle kofaktori pyrrolokinoliinikinoni (PKK) ja mittaamalla sen sähkökemiaa. PKK:ta saatiin adsorboitua suuri määrä ja elektrodilla oli redox-vaste laajalla pH-välillä. Katodilla testattiin metanolia sietäviä, Pt-vapaita typpidoupattuja hiilinanoputkia alkalisessa SMPK:ssa, koska tämän tyyppisiä katalyyttejä ei ollut testattu laajasti näissä olosuhteissa. Uuden katalyytin teho oli ennätyksellisesti 4 kertaa parempi kuin Pt-katalyytin käyttäen ilmaa hapettimena.

Väitöskirjan 2. osassa valmistettiin integroitu kaasudiffuusiokerros Si nanoneulasista (nanoruoho), jota testattiin mikropolttokennossa (MPK). Kerros toimi hyvin alhaisilla virrantiheyksillä. Enemmän tehoa vaativiin sovelluksiin otettiin käyttöön normaali hiilikangas ja nanoruohoa käytettiin vähentämään kontaktivastusta sen ja virtauskanaviston välillä. Nanoruohon käyttö paransi MPK tehoa ja kestävyyttä. Lopuksi MPK:ja käytettiin uusien SMPK-katalyyttien testaamiseen ja tuloksia verrattiin laboratoriokokoisella kennolla saatuihin. Tuloksissa oli eroja, mikä osoittaa, että myös SMPK-komponenteilla on suuri merkitys katalyyttitestauksessa.

Avainsanat suorametanolipolttokenno, hiilinanomateriaalit, mikropolttokennot, katalyyttikerros

ISBN (painettu) 978-952-60-5702-6 **ISBN (pdf)** 978-952-60-5703-3

ISSN-L 1799-4934 **ISSN (painettu)** 1799-4934 **ISSN (pdf)** 1799-4942

Julkaisupaikka Helsinki **Painopaikka** Helsinki **Vuosi** 2014

Sivumäärä 143 **urn** http://urn.fi/URN:ISBN:978-952-60-5703-3

Preface

The work presented in this thesis was carried out at the Department of Chemistry in Aalto University (formerly Helsinki University of Technology) between May 2007 and November 2013. Multidisciplinary Institute of Digitalisation and Energy (MIDE), Fuel Cells and Hydrogen Joint Undertaking (FCH JU), Alfred Kordelin Foundation and Magnus Ehrnrooth Foundation are gratefully acknowledged for financial support of this work.

Firstly, I would like to thank my supervisor, Prof. Kyösti Kontturi, for saying "You should make a Ph.D." in the beginning of things and letting me do it about fuel cells in his laboratory. Together with Dr. Annu Kontturi they have made this place into a brilliant combination of solid scientific work and having fun together. I will never forget the atmosphere here and hope to find something similar in my future places of work. The largest thanks go to my thesis advisor Dr. Tanja Kallio, who has guided me through my research, gotten me the money to do it with and pushed me forward with new ideas when my progress seemed to stall.

Secondly, I have had two co-authors and fellow Ph.D. students who have enabled me to do the fuel cell work I have wanted to do. So a big thanks to Ms. Maryam Borghei for synthesizing all the catalyst materials and to Dr. Gianmario Scotti for fabricating all those micro fuel cells. Without your expertise this thesis would not have reached the level it is now. Seeing how enthusiastically you have done your research has motivated me and your questions of electrochemistry have kept me on my toes. I would also like to thank their supervisors Dr. Virginia Ruiz, Prof. Esko Kauppinen and Prof. Sami Franssila for taking an interest to my work and helping to make the publications better.

I have worked with excellent colleagues in the laboratory over the years. Electrochemistry is a broad subject and each person has had a different perspective on the problems and solutions we had, which has made our research interesting and productive. Especially I would like to thank the Fuel Cell group for their advice, comments and questions: Dr. Ville Saarinen, Dr. Annukka Santasalo-Aarnio, Dr. Pekka Peljo, Dr. Marta Figueiredo and Mr. Sami Tuomi, but not forgetting the other Ph.D. students I have shared my time at Fyke: Dr. Kirsi Yliniemi, Dr. Benjamin Wilson, Dr. Timo Laaksonen, Prof. Päivi Laaksonen, Dr. Marjukka Ikonen, Dr. Outi Toikkanen, Dr. David Lloyd, Lic.Sci. (Tech) Nguyet Doan, Ms. Maija Huuppola, Mr. Tuomas Vainikka, Ms. Elina Pohjalainen, Mr. Lauri Viitala and Mr. Miikka Jokinen. I have had many moments of desperation and joy during my Ph.D. but the most important thing has been to be able to talk, laugh and curse about them with you. Thank you for making my

Ph.D. also the time of my life. Additionally, I would like to thank Ben and Annukka for proof-reading my thesis.

Outside the laboratory, I have also had a good board game group once a week with other people doing their Ph.D.s or working in research. It has been interesting to hear things from other laboratories and how different things can be. Thank you for those splendid evenings when the roll of the dice defined the future Ms. Maiju Laaksonen, Mr. Janne Tynell and especially Dr. Tommi Tynell who has been my good friend since we studied together at TKK and later doing thesis in neighboring labs.

I would also like to thank my family for always believing and supporting me and showing pride in the things I do. Finally, most importantly, thank you Mari for being who you are and making every day the best it can be.

Petri Kanninen
Espoo, February 2014

Contents

List of publications ..... **i**

Author's contributions ..... **ii**

List of abbreviations and symbols ..... **iii**

1. Introduction **1**

2. Direct methanol fuel cell **4**

2.1 DMFC components 4

2.2 Acidic and alkaline DMFC operation 6

2.3 Methanol crossover in DMFC 8

3. Experimental approaches **10**

3.1 3-electrode half cell experiments 10

3.2 MEA preparation 12

3.3 Fuel cell characterization 13

3.4 Ex-situ characterization 15

4. Catalysis in direct methanol fuel cells **17**

4.1 Methanol electro-oxidation 17

4.1.1 Pt-based catalysis 17

4.1.2 Enzymatic catalysis 19

4.1.3 The role of carbon support 23

4.2 Oxygen reduction 26

4.2.1 Pt-based catalysis 26

4.2.2 Nitrogen-modified carbon catalysts 28

5. Fuel cell electrode structure **31**

5.1 3-phase boundary 31

5.2 Membrane-electrode assembly fabrication history 32

5.3 Fabrication of catalyst layers with thin film methods 33

5.3.1 Ionomer content 33

5.3.2 Carbon supports 36

5.3.3 Fabrication techniques 38

5.3.4 Other methods to influence the catalyst layer 42

6. Micro fuel cells **44**

6.1 Micro fuel cell fabrication 44

6.1.1 Optical litography 45

6.1.2 Etching 45
6.1.3 Surface coating 47
6.2 Special constructions for micro fuel cells 48
6.2.1 Gas diffusion layer 48
6.2.2 Silicon nanograss as performance enhancer with a carbon felt GDL 50
6.3 Micro fuel cells as a catalyst thrift tool 52

7. Conclusions 54
7.1 Recommendations for further work 56

References 57

Publications 70

List of publications

This thesis consists of an overview and of the following publications which are referred to in the text by their Roman numerals.

I Petri Kanninen, Virginia Ruiz, Tanja Kallio, I.V. Anoshkin, Esko I. Kauppinen and Kyösti Kontturi: Simple immobilization of pyrroloquinoline quinone on few-walled carbon nanotubes, *Electrochemistry Communications* **12** (2010) 1257-1260.

II Petri Kanninen, Maryam Borghei, Virginia Ruiz, Esko I. Kauppinen and Tanja Kallio: The effect of Nafion content in graphitized carbon nanofiber based anode for the direct methanol fuel cell, *International Journal of Hydrogen Energy* **37** (2012) 19082-19091.

III Petri Kanninen, Maryam Borghei, Olli Sorsa, Elina Pohjalainen, Esko I. Kauppinen, Virginia Ruiz and Tanja Kallio: Highly efficient cathode catalyst layer based on nitrogen-doped carbon nanotubes for the alkaline direct methanol fuel cell, *Applied Catalysis B: Environmental* **156-157** (2014) 341-349.

IV Maryam Borghei, Gianmario Scotti, Petri Kanninen, Timo Weckman, Ilya V. Anoshkin, Albert G. Nasibulin, Sami Franssila, Esko I. Kauppinen, Tanja Kallio and Virginia Ruiz: Enhanced performance of a silicon microfabricated direct methanol fuel cell with PtRu catalysts supported on few-walled carbon nanotubes, *Energy* **65** (2014) 612-620.

V G. Scotti, P. Kanninen, M. Mäkinen, T. Kallio and S. Franssila: Silicon nanograss as micro fuel cell gas diffusion layer, *Micro & Nano Letters* **5** (2010) 382-385.

VI Gianmario Scotti, Petri Kanninen, Tanja Kallio and Sami Franssila: Integration of Carbon Felt Gas Diffusion Layers in Silicon Micro Fuel Cells, *Journal of Micromechanics and Microengineering* **22** (2012) 094006.

Author's contributions

Publication I	The author defined the research plan together with the co-authors and did all the experimental work. He interpreted the results and wrote the manuscript.
Publication II	The author defined the research plan together with the co-authors and did all the experimental work excluding the catalyst synthesis, electron microscopy and XRD analysis. He interpreted the results and wrote the manuscript.
Publication III	The author defined the research plan together with the co-authors. He developed the fuel cell fabrication method and was responsible of the experimental work excluding catalyst synthesis and participated in it actively. He interpreted the results and wrote the manuscript.
Publication IV	The author defined the research plan together with the co-authors and did the fuel cell and contact angle experiments. He had an active role in interpreting the results and writing the manuscript.
Publication V	The author defined the research plan together with the co-authors and did the fuel cell experiments. He had an active role in interpreting the results and writing the manuscript.
Publication VI	The author defined the research plan together with the co-authors and did the fuel cell and contact angle experiments. He had an active role in interpreting the results and writing the manuscript.

Espoo, February 25th, 2014

_____

Prof. Kyösti Kontturi

List of abbreviations and symbols

List of abbreviations

BET	Brunauer-Emmett-Teller theory of adsorption
CE	counter electrode
CL	catalyst layer
CNT	carbon nanotube
CNF	carbon nanofiber
DMFC	direct methanol fuel cell
DHE	dynamic hydrogen reference electrode
DRIE	deep reactive ion etch
EC number	Enzyme Commission number
FAA3	alkaline anion-exchange membrane (brand of Fumatech GmbH)
FWCNT	few-walled carbon nanotube
GDL	gas diffusion layer
GNF	graphitized carbon nanofibers
ITO	indium tin oxide
MEA	membrane-electrode assembly
MEMS	micro electromechanical system
MFC	micro fuel cell
MOR	methanol oxidation reaction
MWCNT	multi-walled carbon nanotube
N-doped	nitrogen-doped
N-FWCNT	nitrogen-doped few-walled carbon nanotubes
NAD	nicotinamide adenine dinucleotide
Nafion®	sulfonated tetrafluoropolyethylene copolymer
OCV	open circuit voltage
ORR	oxygen reduction reaction
PEMFC	polymer electrolyte membrane fuel cell
PF	pore former
PQQ	pyrroloquinoline quinone
PTFE	polytetrafluoroethylene (Teflon®)
RDE	rotating disc electrode
RE	reference electrode

RIE	reactive ion etch
SEM	scanning electron microscopy
SWCNT	single-walled carbon nanotube
TBA^+	tetrabutylammonium cation
TEM	transmission electron microscopy
TMPD	N,N,N',N'-tetramethylphenylene-1,4-diamine
WE	working electrode
XPS	X-ray photoelectron spectroscopy

List of symbols

ε	dielectric constant of a substance
F	Faraday's constant (96485.31 C mol^{-1})
I	current (A)
n	quantity of material (mol)
Q	charge (C)
t	time (s)
z	number of transferred electrons

1. Introduction

The world is becoming increasingly dependent on portable electronic devices, which demand more energy as they become more complex. Lithium ion batteries are widely used as the power sources in these devices due to their light weight and high energy density. However, their recharging is a slow process and as devices become smaller, the batteries themselves must also be reduced in size decreasing the total energy they can store at one time. One promising alternative to batteries are fuel cells: electrochemical power generators that take in fuel like hydrogen, methanol, ethanol or methane to the anode and an oxidant like air to the cathode combining them to produce electricity directly without a combustion step. A fuel cell works as long as there is fuel and air available and "recharging" is a simple exchange or filling of a fuel cartridge that can take only seconds.

The fuel for portable applications should be of high volumetric energy density. Hydrogen or other gases are not optimal for this as they need to be compressed, which complicates a system that needs to be as small and simple as possible. On the other hand, the volumetric energy density of pure methanol (4.3 kWh l^{-1}) is almost twice that of even liquid hydrogen (2.4 kWh l^{-1}), which has led to an extensive study of direct methanol fuel cells (DMFC) using methanol as fuel. However, DMFCs are not yet commercially viable due to their high price, low power and low durability. These problems are related to the complicated oxidation reaction that requires a high loading of precious metal catalyst like Pt at room temperature, the crossover of methanol from anode to cathode and the formation of poisoning or degrading side or intermediate products (*e.g.* CO and H_2O_2). There is an intensive effort to find more active, durable, tolerant and cheaper catalysts for both the methanol oxidation reaction (MOR) and oxygen reduction reaction (ORR).

For MOR, one interesting choice is the utilization of biocatalysts, namely enzymes. Usually enzymes work in solution but for a simplified fuel cell structure it would be advantageous to immobilize them on the electrodes. In **Publication I**, preliminary work to aid this goal was made by immobilizing the cofactor (electron acceptor) of a

methanol oxidizing enzyme on carbon materials and studying the electrochemical properties of the resulting electrode. This structure could be used for enzyme immobilization and to enhance their direct electron transfer properties by using enzymes with their cofactors removed (apoenzymes), which the recombine at the electrode. Few-walled carbon nanotubes (FWCNT) were shown to adsorb a large quantity of the cofactor and produce a strong and durable electrochemical redox response in both neutral and acidic solutions.

The testing of new catalysts for DMFC is often limited to activity and durability test *ex-situ* in a 3-electrode cell. This is a fast way to separate good catalytic activity from bad but it does not necessarily tell how they will behave in the actual DMFC environment as an integral part of the fuel cell is the membrane-electrode assembly (MEA), in which the catalyst material forms a catalyst layer (CL) with a binder that is usually the same material as the membrane is. Furthermore, the CL is in contact with the membrane, whose dimensions change in different conditions adding mechanical stress to the CL. The catalyst and its support can have a substantial influence on the CL structure, thus changing its transport properties for the reactants, ions and electrons. Moreover, the long-term testing of the catalysts is limited to hours in the 3-electrode cell and only concerns the catalyst, while a DMFC system with the MEA should be stable for weeks and months. Even if the catalyst is tested in a DMFC, often only the performance is measured and durability issues are ignored. In this thesis, the focus of the catalyst research has been to study both their long term DMFC behavior and the optimal CL structure. In **Publication II**, the optimum ionomer content of an anode CL was investigated with a previously tested graphitized carbon nanofibers (GNF) supported PtRu catalyst. It was found out that the optimum content was 20-30 wt% higher than with commercial catalysts and performance of the DMFC also increased by 30% between the unoptimized and the optimized CL. This is an important fact to take into account when new catalysts are researched as they may appear less appealing if they are compared against well-studied commercial catalysts under optimum conditions. In **Publication III**, the ionomer content was optimized for a metal-free nitrogen-doped FWCNT ORR catalyst and it was compared against commercial carbon supported Pt in an alkaline DMFC. Even though N-doped carbon has been shown to be as active as Pt in alkaline conditions and also tolerant to methanol crossover, the few fuel cell studies undertaken so far have concentrated either on hydrogen fuel cells or acidic fuel cells and mostly N-doped carbon has not performed as well as Pt. Now that the N-doped FWCNTs were compared with an optimized CL structure in an alkaline DMFC - thus taking advantage of their unique properties - the performance was 4 times better than with Pt.

In addition to the fuel, the size of the actual DMFC should also be miniaturized so it can be integrated for example into smart phones. Micro fuel cells have been under research for the last 15 years with fabrication techniques adapted from the Si semiconductor industry, where microstructures have been important for decades. These techniques are based on the selective etching of Si and can be used to form fuel cell components. One example of a specialized microstructure is Si nanograss, which consists of surface covered with a large number of random Si nanoneedles of less than 2 μm in height. In **Publication V**, this nanograss was used as an integrated gas diffusion layer (GDL) with a cheap Cr protective and conductive layer in a Si micro fuel cell with hydrogen. This was proven to be a feasible solution for reactant distribution in several configurations but at high current densities the performance degraded quickly and irreversibly. It was concluded that such a thin GDL is not suitable for high performance devices. However, the properties of Si nanograss were further studied in **Publication VI**, where it was used as a high surface area contact between a commercial carbon felt GDL used commonly in regular sized fuel cells (thickness 250 μm) in a hydrogen micro fuel cell. It was shown to decrease the contact resistance between the GDL and the Si fuel cell and also improve the water management in the cell during use showing that the components of standard- and microsized fuel cell systems can be used together for improved performance.

All the themes of this thesis were gathered in **Publication IV**, where Si micro-DMFCs with nanograss GDLs were used to study the performance, stability and the anode CL structure with three different carbon supported PtRu catalysts (carbon black, GNF, FWCNT). The small dimensions of the micro-DMFCs enable the use of smaller amounts of experimental catalysts, whose availability can be limited. Significant differences in the CL structure were observed from scanning electron microscopy (SEM) images. The performance results were compared with the test of the same catalyst in a normal laboratory-sized DMFC and it was noticed that also the components outside the MEA have significant influence on the DMFC performance and that if general conclusions are to be drawn from fuel cell testing, the measurement equipment and conditions have to be precisely defined.

In summary, the object of this thesis has been to study the problem areas for portable fuel cells systems. New catalysts for DMFCs based on carbon nanostructures are researched and methods to examine them in relevant ways within the actual system are considered. Also, the alternative microstructures for fuel cell component miniaturization are tested in Si-based cells and they are used as a test platform for the new DMFC catalysts.

2. Direct methanol fuel cell

2.1 DMFC components

A DMFC is a device where the chemical energy of methanol is directly converted to electricity, CO_2 and water. The basic components of a DMFC system are presented in Figure 1, although the structure is the same for all ion-exchange membrane based fuel cells. Methanol is oxidized at the anode, which is usually composed of catalytic, bimetallic PtRu nanoparticles on carbon support, and oxygen is reduced at the cathode, which is usually composed of Pt nanoparticles also on carbon support. More details on the anode and cathode catalysts and reactions are presented in Chapter 4. The binder of the CL is an ion-conducting ionomer, optimally the same material as the electrolyte that prevents the electrodes from short-circuiting. The electrolyte is an ion-conducting but electrically insulating membrane that separates the methanol and the oxygen from each other and forces the electrons to travel through an external electrical circuit. There the electron flow and the potential difference between the anode and the cathode can be converted directly to work. The most common membrane materials consist of a hydrophobic polymer back bone and hydrophilic side chains, which contain dissociating ionic groups (*e.g.* commercial Nafion® in Figure 2). Although the exact microstructure of the membrane is not yet understood completely, the generally accepted model is that the back bones and side chains separate to different phases and ion-conducting pathways are formed inside the membrane from the hydrophilic side chains [1].

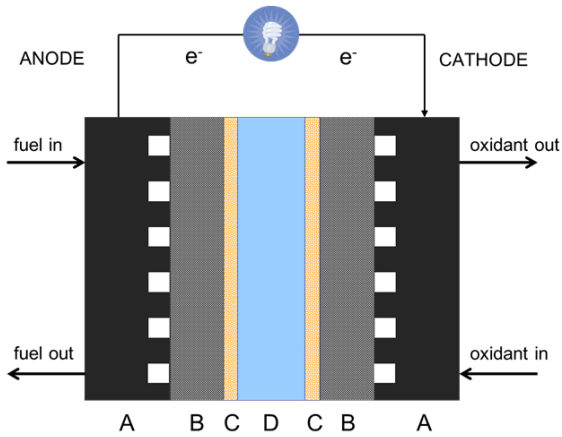

Figure 1. The basic schematics of a DMFC system. A) current collectors with flow fields, B) gas diffusion layers, C) catalyst layers and D) electrolyte.

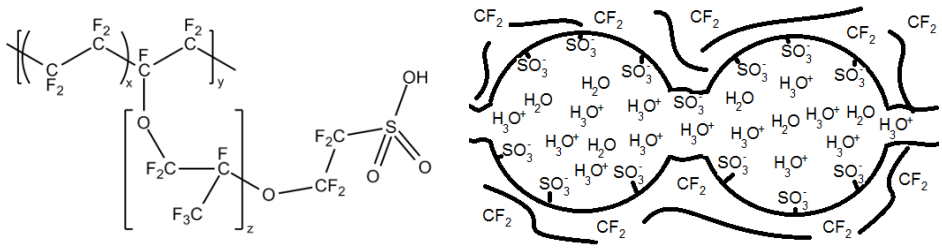

Figure 2. The molecular and a proposed cluster microstructure of Nafion. The diameter of the hydrophilic clusters are 2-5 nm depending on the hydration state of membrane (the wetter the membrane, the larger the cluster). [1]

Important factors for DMFCs are the distribution of reactants to the CL and the removal of reaction products from the system. First, the reactants are delivered into the system through a flow-channel, which can have various geometries: serpentine and parallel channels are most common (Figure 3) [2]. The shape of the channel cross-section is generally rectangular. Due to the ridges of the flow channel, a diffusion layer is required between the ridge and the CL so that flow to the whole catalyst area is unobstructed. Most common diffusion layers are carbon paper, felt and cloth with a hydrophobic polytetrafluoroethylene (PTFE) coating to ensure pathways for gaseous substances to reach and leave the active sites, while liquid is present (*e.g.* O_2 in water or CO_2 in methanol) [3].

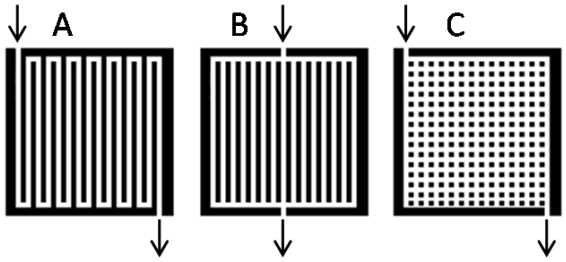

Figure 3. Examples of flow channel geometries employed in fuel cells. A) serpentine, B) parallel and C) pillar type.

2.2 Acidic and alkaline DMFC operation

A DMFC can be operated either in acidic or alkaline mode depending on the ion-conducting membrane material used. If it is cation-conducting, the fuel cell operates in acidic mode and the transported ion is the proton (H^+). If it is anion-conducting, the fuel cell operates in alkaline mode and the transported ion is the hydroxide (OH^-). The electrode reactions and their thermodynamical potentials are:

ACIDIC

Anode:	$CH_3OH + H_2O \rightarrow CO_2 + 6H^+ + 6e^-$	E^o=-0.015 V	(i)
Cathode:	$\frac{3}{2}O_2 + 6H^+ + 6e^- \rightarrow 3H_2O$	E^o=1.228 V	(ii)
Total:	$CH_3OH + \frac{3}{2}O_2 \rightarrow CO_2 + 2H_2O$	E^o=1.213 V	(iii)

ALKALINE

Anode:	$CH_3OH + 6OH^- \rightarrow CO_2 + 5H_2O + 6e^-$	E^o=0.814 V	(iv)
Cathode:	$\frac{3}{2}O_2 + 3H_2O + 6e^- \rightarrow 6OH^-$	E^o=0.399 V	(v)
Total:	$CH_3OH + \frac{3}{2}O_2 \rightarrow CO_2 + 2H_2O$	E^o=1.213 V	(vi)

It can be seen that even though the electrode reactions change, the total cell reaction stays the same and thus, the thermodynamical potential of the DMFC is the same both in acid and alkaline. The processes occurring in both cell types are illustrated in Figure 4.

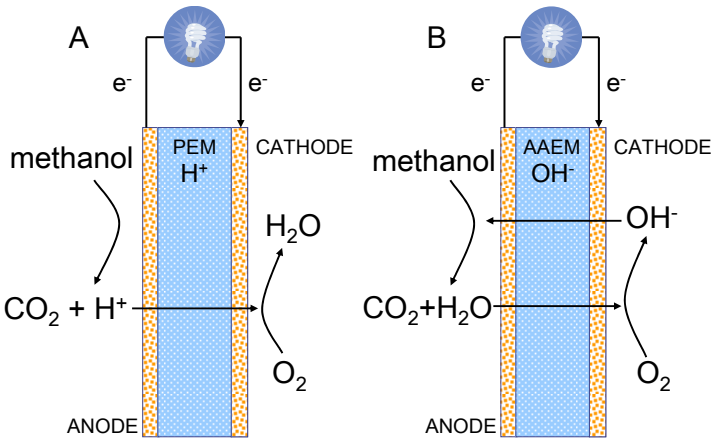

Figure 4. The operation principle of A) acidic and B) alkaline DMFC.

There are several advantageous and disadvantageous features for both the acidic and alkaline DMFC. The acidic DMFC has been studied more extensively and currently can attain more than 10 times higher current and power densities when compared to the alkaline version [4]: the highest maximum power densities obtained from single cell alkaline DMFCs without aqueous electrolyte and with air oxidant at 60°C are around 10 mW cm^{-2} [5] while acidic DMFCs can operate at 100-200 mW cm^{-2} [6]. Part of the difference is explained by the relative novelty of the alkaline membrane fuel cells as their development has only started this century [7], while acidic Nafion-based fuel cell have developed since 1960s [8]. Another part of the performance difference comes from the fact that protons have almost double the molar conductivity compared to hydroxide ions (349 and 198 S cm^2 mol^{-1}, respectively [9]). These are fundamental properties that cannot be changed, so the most straightforward way to improve the conductance of an alkaline membrane is to make it thinner. However, acidic membranes are based on perfluorinated or hydrocarbon and are quite robust, so making the alkaline membranes thinner is difficult. The performance of an alkaline DMFC can be improved by adding an alkaline substance (*e.g.* KOH or NaOH) into the feed methanol solution [10], but this introduces the risk of carbonate precipitation into the system. Carbonate is formed from the anode reaction where CO_2 is produced with the following reaction :

$$CO_2 + 2OH^- \rightarrow CO_3^{2-} + H_2O \qquad \text{(vii)}$$

The produced carbonate can react with the cations from the added base to form precipitates, which can block the pores of the CL and decreases the basicity of the solution [11]. However, this is exactly the problem that is trying to be avoided by using

the solid alkaline electrolyte with fixed cationic groups instead of the aqueous electrolyte in the traditional alkaline fuel cells and is therefore not a recommended practice. The disadvantage of carbonation for the alkaline membrane is the decreased basicity of the anode, which causes a pH difference over the membrane resulting in a thermodynamical potential loss in the cell [12]. Furthermore, because the pH is closer to neutral, the reaction rate slows down as it is H^+/OH^- dependent [13]. The membrane can also be carbonated, even by exposure to ambient air, which decreases the conductivity [14] (the molar conductivity of carbonate ions is 139 S cm^2 mol^{-1} [9]).

The main advantage of the alkaline DMFC is the possibility to use non-Pt catalysts at the electrodes, *e.g.* Ni for MOR [15] and Ag [16], nitrogen-modified carbon (Publication III) or perovskites [17] for ORR, which are also less prone to poisoning by methanol crossover than Pt. Another important factor is the hydroxide ion flow from cathode to anode that reduces the methanol crossover compared to acidic DMFC where protons transport methanol to the cathode *via* electro-osmotic drag (Figure 4). There is no flooding problem at the alkaline DMFC cathode since water is consumed there unlike in acidic DMFC, where water is formed and can block the catalyst sites from oxygen. As water is a stoichiometric reactant at the cathode, it should be kept suitably humid, which is usually achieved with the humidifying effect of the water/methanol solution at the anode. In addition, the perfluorinated membranes commonly used in acidic DMFCs (*e.g.* Nafion) are difficult and expensive to fabricate due to harsh synthesis conditions, while alkaline membranes can be made in milder conditions.

2.3 Methanol crossover in DMFC

As methanol is a small, polar and neutral molecule, it can easily penetrate the ion-exchange membrane along with water and protons [18] and it is transported to the cathode due to concentration and pressure gradients over the membrane and by the electro-osmotic drag induced by the proton flow in the acidic DMFC [19]. When methanol reaches the cathode, it is instantly oxidized in the high potential releasing electrons causing oxidative current and electrode depolarization, that is the cathode and thus the cell voltage is decreased. In the process, the cathode catalyst can also be poisoned as CO is produced (see Chapter 4.1.1). The electrons in this case do not travel through an external circuit and cannot be used for useful work.

Methanol crossover is a severe limitation for the DMFC, as it reduces its open circuit voltage (OCV) to less than 0.8 V [20-22] resulting in fuel and catalytic activity loss. Due to the low power and good humidification of the DMFC when compared to H_2-fueled polymer electrolyte membrane fuel cell (H_2-PEMFC), high operating temperatures enhancing the electrode reaction rates are desired but the crossover is also increased

with temperature [23]. Therefore, many efforts have been made to reduce the crossover or to mitigate its effects. As the diffusion through the membrane is partly obeying the Fick's law due to the concentration difference over the membrane, the simplest solution is to use a thicker membrane. However, as the membrane gets thicker, its resistance also increases, so the ohmic losses also increase even though the crossover decreases. A thicker membrane also means larger absolute swelling due to solvent absorption [24], which can cause durability issues in fuel cells as the CL may erode.

Crossover can also be decreased by using a lower concentration of methanol in water at the anode. With Nafion, the optimum methanol concentration is between 1-2 mol dm^{-3} [22,25,26], which means the methanol content is quite low and the water content high. This is inconvenient for practical portable applications as it would be beneficial to minimize the volume and the weight of the fuel solution. In some cases internal dilution has been achieved by using the water produced at the cathode to dilute a high concentration methanol feed [27].

As the increase of the membrane thickness and decrease of the methanol concentration have unwanted side effects, new materials are designed to reduce the methanol crossover and its impact. The cathode catalyst can be modified so that it is not active for MOR or poisoned by CO, thus decreasing the cathode depolarization and increasing the ORR activity (like nitrogen-modified carbon materials (Publication III), Fe porphyrins [28] or transition metal sulfides [29]. A large effort has been directed in designing new membrane materials that would have high conductivity with good mechanical stability and selectivity toward water and protons [18]. The membrane material should also be available in dispersion form so that it can easily be used as the CL binder. As discussed in Chapter 2.2, the use of alkaline membranes is beneficial against the crossover as the flow of ions is reversed from the acidic case, which implies that the electro-osmotic drag actually decreases the methanol transport to the cathode. Also, the choice of methanol and CO tolerant catalysts are larger in alkaline environment.

3. Experimental approaches

3.1 3-electrode half cell experiments

Fuel cell catalyst testing in actual fuel cells requires a relatively large amount of catalyst (10s of milligrams) as well as complicated equipment to house the DMFC components and to control conditions in the cell. Fabricating a MEA can also be a demanding task if the properties of the new material differ from those previously tested. Therefore, it is advantageous to screen new catalysts with simpler methods for catalytic activity and only choose the most promising ones for fuel cell testing. This is done in an electrochemical half-cell (Figure 5) where the amount of required catalyst is small (fraction of a milligram), preparation of the electrode faster and testing of the activity better controlled. The system consists of a working electrode (WE), where the catalyst is deposited and the studied reaction occurs, a counter electrode (CE), where a balancing redox reaction takes place, and a reference electrode (RE), which is kept in constant conditions in a separate container connected to the actual cell through a Luggin capillary. All the current flows between the WE and CE and the potential at the WE is measured against RE, so the voltage and current in the cell can be accurately controlled and measured by a potentiostat. In addition the mouth of the Luggin capillary is placed very close to the WE to minimize the Ohmic losses in the cell. The mostly commonly used WE is a planar glassy carbon electrode, since it has good compatibility with carbon supported catalysts and it is essentially electrochemically inert unlike a Pt electrode. On the other hand, the CE electrode should react quickly because all the current flows through it, so a large Pt electrode is usually used. The choice of the reference electrode depends on the electrolyte: a saturated calomel electrode or Ag/AgCl in KCl is typically used in acidic conditions and the Hg/HgO electrode in alkaline conditions.

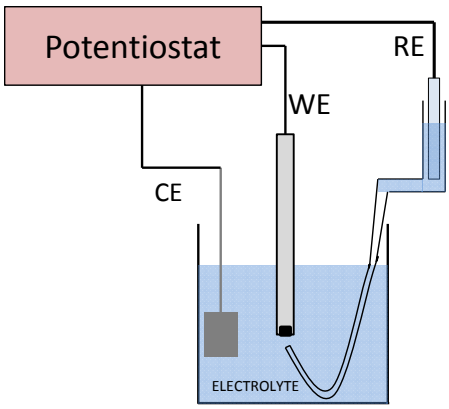

Figure 5. Schematics of a 3-electrode electrochemical cell with a planar working electrode, (WE), platinum wire counter electrode (CE) and a reference electrode (RE).

The most common measurements performed in a 3-electrode cell are cyclic voltammetry to study the catalytic activity and chronoamperometry or chronopotentiometry to study the durability and poisoning effects. In cyclic voltammetry, the voltage of the WE is swept to a certain potential and back, and the current is measured. The onset potential of an irreversible reaction can be determined from the point where a noticeable current starts to flow, or the formal potential of a reversible or quasireversible reaction from the peak current potentials of the anodic and cathodic reactions. The activity of the catalyst can be determined from the level of the current or in the case of immobilized film, the amount of electroactive species from the amount of transferred charge. In chronoamperometry and chronopotentiometry, the voltage and the current, respectively, are set to a value, where the studied reaction takes place, and the other quantity is measured as the function of time. Possible changes in the catalyst, like poisoning or degradation, will show as decrease in the current. The 3-electrode cell can be combined with various surface specific spectrometric techniques that can yield detailed information about the catalyst, reaction pathways and products (e.g. infra-red [30] or X-ray absorption spectroscopy [31]. In Publication I, this set-up was combined with a spectrometer so the changes in the light absorbance of the redox species could be followed as it was oxidized and reduced.

Cyclic voltammograms in 3-electrode cells are also useful in determining the adsorbed amount of an electrochemically active species. Unlike in solution, all of the material is oxidized or reduced when the potential is swept past its formal potential and its amount can be calculated from the transferred current under the redox peaks by Faraday's law if the number of transferred electrons is known:

$$n = \frac{It}{zF} = \frac{Q}{zF}, \qquad \text{(viii)}$$

where I is current, t time, z number of electrons and F Faraday's constant.

This can be used to estimate the electrochemically active surface area of Pt based catalysts as the charge per area of the oxidation of a CO monolayer on Pt is known (420 mC cm^{-2}) [32].

In Publication I, this method has been used to study the interactions of an immobilized film of a common alcohol oxidizing enzyme cofactor, pyrroloquinoline quinone (PQQ), with FWCNTs. Although the method has not been used directly with the new catalyst materials in Publications II, III and IV, all the catalysts were first examined in a 3-electrode cell in previous studies [33,34]. The CO adsorption method was used in the DMFC environment in Publication II to determine the electrochemically active surface area of a MEA [35].

3.2 MEA preparation

The self-made MEAs used in this thesis were made by the thin-film method (Chapter 5.2) [36]. In the case of Nafion MEAs used in Publications II and IV, the catalyst was mixed with Nafion ionomer, isopropanol and water by a magnetic stirrer and, in the case of commercial catalysts, sonicated to form the catalyst ink, which was then sprayed with an airbrush to a pretreated Nafion membrane. This was repeated for both the anode and cathode side. Nafion pretreatment involved boiling the membrane first in 5 vol% H_2O_2, then in 0.5 M H_2SO_4 and finally twice in deionized water. Finally, the MEA was hot-pressed at 130°C with 50 bars for 2 min and assembled in the fuel cell with 10 wt% PTFE-proofed carbon cloth on the anode and 60 wt% PTFE-proofed carbon cloth on the cathode. In Publication V, a slightly modified version of the method was used: methanol was used as the solvent for the ink and the hot-press temperature was 140°C.

In the case of the alkaline MEA used in Publication III, the catalyst was mixed with Fumatech FAA3 ionomer and isopropanol by a magnetic stirrer and sonicator. The ink was then sprayed with an airbrush on to the microporous carbon layer side of Fuel Cell Etc GDL-CT carbon cloth at an elevated temperature of approximately 140°C in order to increase the evaporation rate of the N-methyl-2-pyrrolidone (NMP, boiling point, 202°C) solvent in the ionomer solution. The high temperature was used after the manufacturer (Fumatech) communicated that the ionomer could be subjected to high temperatures (up to 150°C) for short times despite product description. The anode used

in this study was a FuelCellEtc HL2GDE carbon cloth with a 4 mg cm^{-2} PtRu black loading that was covered with approximately 0.30 mg cm^{-2} of the FAA3 ionomer sprayed at 140°C. These electrodes were exchanged to OH- form by placing 1 M NaOH solution on the catalyst surface for 2 h so that the solution was refreshed after 1 h. The FAA3 membrane was pretreated by mixing in a 0.5 M NaOH solution for 1 h followed by mixing in deionized water twice for 30 min at a time. The fuel cell was assembled with these components without hot-pressing, since it has been shown that high pressure combined with temperature degrades the membrane [37].

The MEA used in Publication VI was commercial Gore Primea MEA containing Gore Select membrane, which was used for the high performance characteristics of the membrane [38] and for better reproducibility of the mass fabricated MEA. The membrane is reinforced with a PTFE framework, so it can be manufactured with very low thickness (30 μm) while retaining high mechanical durability.

3.3 Fuel cell characterization

The most important difference of the DMFC measurements compared to the 3-electrode cell in this thesis is that the DMFC does not have a reference electrode. Consequently, the voltage is measured between the WE and CE, *i.e.* the anode and the cathode, and the current also flows through them both. This makes it impossible to determine the exact potential of the WE as the potential of both of the electrodes is changing and only their difference can be measured. However, it is possible to connect, for example, a Pt wire to the membrane surface on the examined side of the cell outside the active area and surround it in a hydrogen gas sheath. As long as the hydrogen partial pressure around the Pt wire remains constant, the electrode is at constant potential and can be used as a reference electrode. Then the voltage measured is between the examined electrode and the membrane. A simpler technique in the case of DMFC anode studies is to replace oxygen or air at the cathode with hydrogen, since the activation overpotential of hydrogen on Pt is much smaller than that of oxygen, and assume that the cathode stays approximately at the same potential even if current is flowing through it. This is called the dynamic hydrogen reference electrode (DHE).

Since a fuel cell is a type of an electrochemical cell, the measurements are similar to that of a 3-electrode cell. The overall performance of a DMFC can be measured with a potential sweep from the OCV to a desired lower potential. This is often called a polarization curve and parameters like maximum power density and current densities at certain potentials can easily be determined from it. The shape of the polarization curve can be used to determine the effect of different energy loss mechanisms called activation, ohmic and mass transfer overpotentials (Figure 6) [39].

Activation losses are defined as the difference between the thermodynamical potential where a reaction should be favorable and the potential where reaction current can be measured. It is a measure of slowness of the reaction and it can be affected by the catalyst choice. When the potential of the cell is reduced further from OCV, the electrodes become polarized, current increases and Ohmic losses become prevalent. This is simply a result of the total resistance of fuel cell and other components in the electrical system. Finally, when the current is increased even further, the concentrations of reactants at the catalyst surface starts to drop as mass transfer cannot counter-balance the matter consumed in the electrode reactions and this shows as an exponential voltage drop. Especially in acidic fuel cells mass transfer can also be hindered because of excess water production at the cathode, which will block the catalyst sites and cause a similar exponential voltage loss at high current densities. The porosity and hydrophobicity of the CL and GDL are important factors in determining the effectiveness of mass transfer to and from the active sites. The effect of water production can be further studied by a cyclic voltammetry measurement, where the voltage scan is continued back to OCV from low potentials (Publication VI). If the backward reverse scan shows lower current densities, it is likely that the excess water generated at the low potentials disturbs the cell performance. On the other hand, if the reverse scan shows higher currents, it is likely that the excess water hydrates the membrane and increases it conductivity.

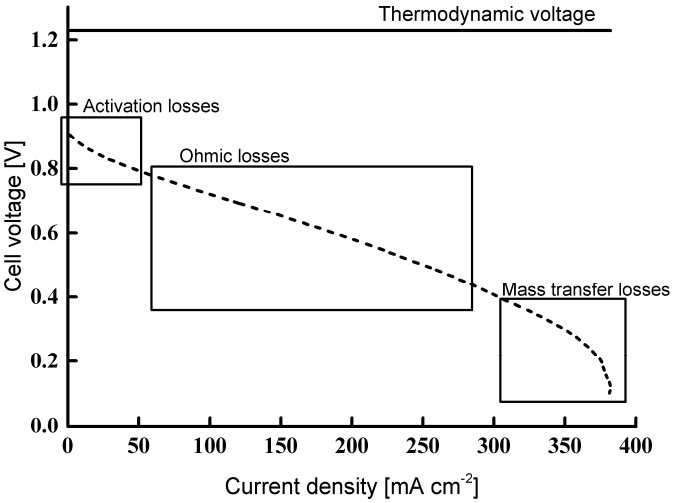

Figure 6. A typical polarization curve of a fuel cell with the different mechanisms of power loss marked. Adapted from Publication VI.

Fuel cell durability is studied with chronoamperometric (Publications III, IV, VI) and chronopotentiometric measurements (Publication II). The durability is usually

measured on much longer time scales than with the 3-electrode cell (minutes versus days) and the most important information gathered are the changes in the catalyst and the CL. These are usually studied electrochemically through the fuel cell performance, by measuring the electrochemically active surface area and by microscopic techniques. The difference between an amperometric (constant voltage) and a potentiometric measurement (constant current) is that with constant current the reactant consumption and product production stay constant during the measurement. Thus, it is more clear that performance changes are related to changes in the fuel cell component structure and not because the reactant and product flows change. The potential of the electrodes changes but this is also true with a constant voltage measurement since the voltage is the difference of the anode and the cathode potential leaving the individual potentials subject to change.

The electrochemically active surface area of Pt-based fuel cell electrode can also be measured, when a reference electrode is used or the one of the electrodes is used as a DHE. On the studied electrode, first nitrogen is used to clean it of other reactive gases, then the area can either be determined from the H adsorption region for Pt or CO adsorption can be used for PtRu (Publication II).

In electrochemical impedance spectroscopy, the fuel cell is excited by an alternating voltage and resulting current is measured or alternating current is used and voltage is measured. Impedance is defined as the ratio of voltage and current. When the frequency of the signal is changed, different processes in the system become dominant. At very high frequencies (>100 kHz), the chemical processes are too slow to affect the impedance and the real resistance of the whole system can be determined (including electrolyte, electrode, wire and contact resistances). At lower frequencies (100 kHz -1 Hz), the electrode reactions cause capacitive and resistive effects and kinetic reaction parameters can be determined from them. At even lower frequencies (<1 Hz), the diffusion effects start to show as Warburg impedances and from which diffusion coefficients can be calculated. Generally, the physical values for the different processes are obtained by a fit to an equivalent circuit containing all the equivalent components of the expected chemical and electrochemical processes. Impedance spectroscopy was used in this thesis to determine the total cell resistances as the measurements were too noisy to allow fitting of the kinetic parameters (Publications II and III)

3.4 Ex-situ characterization

It is often useful to study the MEA outside the fuel cell to better understand its structure and properties. Transmission electron microscopy (TEM) can be used to determine the size of the catalyst nanoparticles and the state of the carbon support

(Publications II, III and IV). SEM is very useful to study the CL structure and thickness from a cross-section sample (Publications II, III and IV). These microscopic techniques are usually destructive to the MEA, so different samples have to be prepared to compare the MEA and the catalyst before and after fuel cell testing.

Contact angle measurements on the MEA surface can be used to probe the hydrophobicity of the CL (Publications II and IV) or the wetting properties of the flow field (Publication VI). Generally a hydrophobic cathode, especially in acidic conditions, is desired as the pathways in the CL can stay open for O_2 transports even with excess water. The measurements should be done on a fully hydrated MEA as the ionomer absorbs water and expands changing the surface properties. If the CL is highly hydrophobic, hydration may take several hours of boiling in water.

As the conductivity of carbon materials are several orders of magnitude higher than the ionomer conductivities, conductivity of the whole CL can be used to probe how well the carbon parts are connected to each other (Publication II). When the amount of ionomer is increased, it usually isolates more carbon support from each other, hindering the electron transfer to and from the current collectors.

4. Catalysis in direct methanol fuel cells

4.1 Methanol electro-oxidation

4.1.1 Pt-based catalysis

The electro-oxidation of methanol on Pt is a complicated procedure [13] but compared to other alcohols it is relatively straight-forward due to the lack of a carbon-carbon bond in its structure. The main oxidation pathways and products in both acidic and alkaline environment are presented in Figure 7. It is immediately clear that water has an important role in the total oxidation of methanol to CO_2.

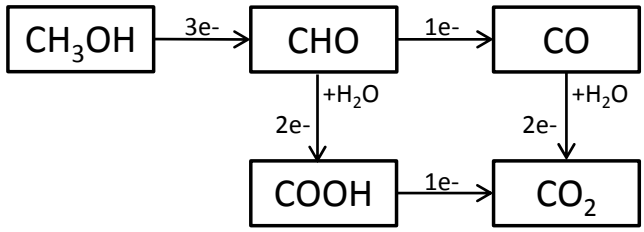

Figure 7. Simplified MOR pathways to intermediate and final products on Pt surface. Arrows present the loss of the total 6 electrodes possible to extract from methanol oxidation.

Oxidation starts with the adsorption of methanol to the Pt surface as all the reactions happen on the surface [40]. The hydrogens are then removed from the carbon and the oxygen so that reactive species formyl is left:

$$CH_3OH_{ads} \rightarrow CH_2OH_{ads} + H^+ + e^- \quad \text{(ix)}$$

$$CH_2OH_{ads} \rightarrow CHOH_{ads} + H^+ + e^- \quad \text{(x)}$$

$$CH_2OH_{ads} \rightarrow H_2CO_{ads} + H^+ + e^- \quad \text{(xi)}$$

$$H_2CO_{ads} \rightarrow CHO_{ads} + H^+ + e^- \quad \text{(xii)}$$

$$CHOH_{ads} \rightarrow CHO_{ads} + H^+ + e^- \quad \text{(xiii)}$$

The oxidation can now take two pathways. In the first case, the formyl is oxidized to CO, which is a poisoning intermediate on Pt as adsorbed water is required to oxidize it further to CO_2:

$$CHO_{ads} \rightarrow CO_{ads} + H^+ + e^- \quad \text{(xiv)}$$
$$H_2O_{ads} \rightarrow OH_{ads} + H^+ + e^- \quad \text{(xv)}$$
$$CO_{ads} + OH_{ads} \rightarrow CO_2 + H^+ + e^- \quad \text{(xvi)}$$

In the other pathway, the formyl reacts first with adsorbed water to form formic acid which is then oxidized to CO_2:

$$CHO_{ads} + OH_{ads} \rightarrow COOH_{ads} + H^+ + e^- \quad \text{(xvii)}$$
$$COOH_{ads} \rightarrow CO_2 + H^+ + e^- \quad \text{(xviii)}$$

Methanol, formaldehyde and formic acid can also desorb from Pt and return to the solution before oxidation proceeds and adsorb again. The exact details of the mechanism, rate determining step and activity vary according to conditions and the crystal structure of the Pt surface (commonly a polyoriented nanoparticle) [41]. For the alkaline environment, the mechanism is similar: formyl is the splitting point of the pathways with the exception that the hydrogen bonded with oxygen is removed first and then the carbon-bonded hydrogens. Due to the alkaline environment, formate (COO^-) and carbonate species (CO_3^{2-}, HCO_3^-) are present.

$$CH_3OH_{ads} \rightarrow CH_3O_{ads} + H^+ + e^- \quad \text{(xix)}$$

As can be seen from the reactions, the key factor for complete oxidation and removal of products is the adsorption of water to Pt. However, this is not a favored process on Pt and only happens at potentials more positive than 0.4 V vs RHE in acid [42,43] and alkaline [44,45]. In order for the reactions to proceed, the anode potential has to be higher than this which decreases the total cell voltage. To solve this problem, Pt has been used with other metals that favor water dissociation and adsorption at lower potentials thus supplying the MOR products on Pt sites with adsorbed OH (bifunctional effect). As CO and OH are required to be at adjacent sites to react, its efficiency depends on the surface diffusion of species. This has been shown to be a fast process for CO on Pt [46,47]. Many metals have been used to form bimetallic catalysts with Pt and enhance its catalytic properties for methanol electro-oxidation, like W, Sn and Mo [48]; Sn [49]; Pd, Sn [50]; Os [51]; Fe, Co, Ni, Cu [52]; Co [53] and Ni [54] or even tri- and tetrametallic systems [48,55,56]. However, the state-of-the-art option is Ru, which was introduced already in the 1960s [57] and is commonly used in commercial catalysts and as the standard catalyst in DMFC testing. Due to the lower OH adsorption potential of

Ru, the onset potential of MOR can be lowered by 0.15 V at operational DMFC temperatures (80°C) [42]. It also enhances the catalytic properties of Pt via the so called ligand effect, which means it changes the electronic structure of Pt and reduces the Pt-CO bond energy so that the surface diffusion is facilitated [47]. Moreover, selectivity of methanol oxidation to CO_2 is very high with PtRu catalyst, more than 95% [58-60]. Due to the easily oxidized nature of Ru, its dissolution is one of the main decay mechanisms in DMFC [61], but this can be mitigated with different carbon supports, like carbon nanotubes (CNT) [62] or by nitrogen-doping carbon (N-doped carbon) [63,64].

4.1.2 Enzymatic catalysis

Enzymes are proteins that catalyze metabolic reactions in living organisms. They have a complex 3D structure based on the folding of the primary amino acid chain making them highly selective, while this also makes them very sensitive towards the environment as small changes in the temperature and pH can deactivate them permanently. However, it is possible to isolate enzymes from cells and use them as high activity biocatalyst at ambient temperatures.

Methanol can be oxidized by variety of enzymes derived from different species but especially interesting for practical applications are quinoproteins characterized by a quinone cofactor (an electron receptor, *e.g.* PQQ, tryptophan tryptophylquinone, topaquinone or lysine tyrosylquinone) [65]. For methanol, the oxidizing enzyme is called methanol dehydrogenase which contains two PQQ cofactors (Enzyme commission (EC) number 1.1.2.7). This enzyme can be derived from various bacteria with slightly differing structures and it oxidizes methanol to formaldehyde or formic acid. The electrons from methanol are first transferred to the cofactor and can then be moved forward to external targets in two alternative ways: by mediated electron transfer or by direct electron transfer. The cofactor is tightly bound inside the enzyme, so its presence outside the enzyme is not required and the enzyme is active simply by insertion into a suitable environment. The reduction and oxidation reactions of PQQ are presented in Figure 8.

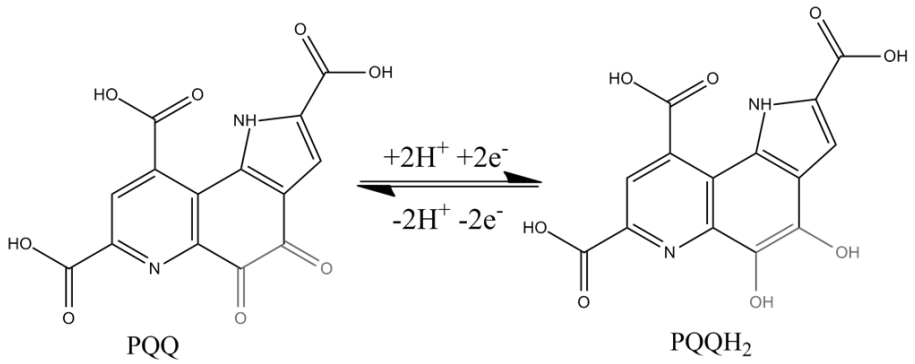

Figure 8. The molecular structure of oxidized and reduced PQQ.

In mediated electron transfer, the system contains species whose formal potential is above that of the cofactor and which can interact with the enzyme. The electrons are transferred by chemical reduction to the mediator, which will at some point arrive to the electrode, reoxidize there and return to be reduced once again by the cofactor [66-68]. A common example used with PQQ-based enzymes is N,N,N',N'-tetramethylphenylene-1,4-diamine (TMPD) [68]. The most important parameter is the formal potential difference between the cofactor and the mediator because that potential difference is lost for the fuel cell. The situation is similar when the cofactor of the enzyme is mobile, like nicotinamide adenine dinucleotide (NAD), and transports the electrons from the enzyme to the electrode. Due to the sluggish redox reactions of NAD, the electrode surface is modified with *e.g.* methylene green [69], Nile blue and 4-carboxyphenyl boronic acid [70], polyamidoamine dendrimers with [71] and without MWCNTs [72]. These examples are of ethanol fuel cells but the same enzymes can be applied to DMFCs (EC number 1.1.1.1) [73].

In direct electron transfer, the electrons move directly from inside the enzyme to the electrode without diffusing intermediates. This requires the use of a bound cofactor like PQQ. There are two examples of ethanol fuel cells using this method. Ramanavicius *et al.* [74] used gluteraldehyde to immobilize alcohol dehydrogenase on to a graphite electrode but the resulting fuel cell had very low power density of 1.5 μW cm^{-2}. Neto *et al.* [75] immobilized the same enzyme and an aldehyde dehydrogenase with a composite of Nafion and MWCNTs and could improve the maximum power density of the cell to 38 μW cm^{-2}. These power values are small compared to the few hundreds of μW cm^{-2} achievable with NAD-based enzymatic ethanol fuel cells [70,72] but the simplified system with less species in the solution and fixed catalyst like the metal catalyst in H_2-PEMFCs and DMFCs justifies the continued research for improved performance. However, direct electron transfer has been used for several alcohol biosensor applications using enzyme immobilization via *e.g.* organic salts in silicon oil [76], osmium complexes [77], conducting polymers [78] or thiol layer [79] showing the

viability of direct electron transfer with PQQ-based enzymes. In these cases, the electrons mostly do not move directly from PQQ to the electrode but travel through *heme-c* redox groups inside the enzyme [78].

Considering the direct electrochemistry of PQQ, the use of apo-enzymes (that is enzymes with the PQQ cofactor removed) is important as they can reconstitute on the PQQ, thus forming a good electrical connection between the enzyme and the electrode [80,81]. Several studies of the electrochemistry of immobilized PQQ can be found from the literature. Shinohara *et al.* [82] modified a Pt electrode with a film of conducting polymer polypyrrole and performed the polymerization in the presence of PQQ effectively trapping it in the polymer film. The immobilized PQQ showed quasireversible behavior and moderate stability over 6 h. This stability could be enhanced by employing a thicker polypyrrole film indicating that PQQ was gradually leaching out. Similarly, Curulli *et al.* [83] coated Pt, Au and graphite electrodes with non-conductive polyaminobenzene in the presence of PQQ and measured more reversible behavior than with coated electrodes and free PQQ. Katz *et al.* [84] modified Au electrode with cystamine to covalently bond the PQQ to the electrode via carbodiimide coupling to one of its carboxylic acid group. The redox reaction was faster at high pH possibly indicating favorable interactions between the negatively charged PQQ and the remaining cystamine layer. Yamashita *et al.* [85] used Zr modified silica gel to immobilize PQQ and studied its electrochemical properties with a carbon paste electrode. PQQ oxidation peak was split in two at pH above 3 but in acidic conditions the reaction proceeded more reversibly. Jao *et al.* [86] used didodecyldimethylammonium bromide modified indium tin oxide (ITO) glass and immobilized PQQ there by potential cycling. These electrodes showed PQQ redox peaks at pH < 8.55 and response optimum was at around pH 3. They connected this with the PQQ form prevalent at pH 3 with two carboxylic acid groups next to nitrogen atoms deprotonated and the nitrogen in the pyridine ring protonated.

These methods are somewhat cumbersome and the electrode is not optimized for high surface concentration of PQQ. This is not a problem for sensor application as even small currents can be used to detect different concentrations but for fuel cells the goal is to extract as much current and power as possible. This means that the enzyme concentration should be large. In Publication I, the goal was to immobilize PQQ on carbon materials (carbon black, single-walled carbon nanotubes (SWCNT), FWCNTs) on glassy-carbon electrodes with a simple method and at large quantities for possible use in enzymatic methanol fuel cells and electrolyser. FWCNTs, which are small multi-walled carbon nanotubes (MWCNT) with 2-5 walls (~3-9 nm in diameter, 1 μm in length) [87], have unique properties that combine the robustness of MWCNTs and the structural perfection of SWCNTs [88]. For example, the outmost wall can be

functionalized without the loss of conductivity because the inner walls are intact, while minimizing the volume of the CNTs. The same FWCNTs were used also in Publications II, III and IV.

The carbon materials were simply deposited from dispersions and dried. PQQ was deposited by immersing the electrodes in PQQ solution (in phosphate buffer of pH 9.5) for 2 h and washing any free PQQ away from the electrode. With electrodes fabricated this way, it was found that FWCNTs absorbed 30 times more PQQ per gram than the other materials and therefore, it was selected for further studies at different pH values. This is likely due to FWCNT forming agglomerated spots on the electrode, which can contain more PQQ than homogenous thin layers formed from SWCNTs and carbon black. The FWCNT-PQQ electrode showed a well-defined electrochemical response in wide pH windows from pH 2 to 12 and it was almost completely stable for 515 potential cycles at pH < 6 (Figure 9). Peak splitting seen by Yamashita *et al.* [85] was only evident at pH 12 or at higher voltage scan speeds (50 mV s^{-1}) and the pH window for the electrochemical response was wider than achieved by Jao *et al.* [86]. The electrode was also more stable than the electrodes fabricated by Shinohara *et al.* [84] and Katz *et al.* [82] at pH 7 most likely due to π–π stacking between the aromatic rings of the FWCNTs and the PQQ [89,90]. However, electrostatic effects controlled strongly both the immobilization and the stability of the electrode. FWCNTs were functionalized by acid treatment which introduces oxygen containing groups to their surface, among others –OH and –COOH. These can deprotonate in alkaline solution as can the –COOH and –NH in the PQQ. This increased negative charge in the molecules causes electrostatic repulsion that decreases both the deposited amount of PQQ and the electrode stability. This effect was quite dramatic as when the immobilization pH was changed from 9.5 to 2, the amount of the immobilized PQQ halved. The stability of the electrode against the pH of the measurement solution (Figure 9b) could be fitted with the deprotonation degree of a system with two acid constants of 7.6 and 10.8, which coincides well with expected pKa values of –COOH (6.45 [91]) and –OH (>10 [92]) on graphitic surface. In conclusion, Publication I presents a simple way to immobilized large amount of PQQ on a biofriendly carbon surface for possible applications in enzyme immobilization and biocatalysis.

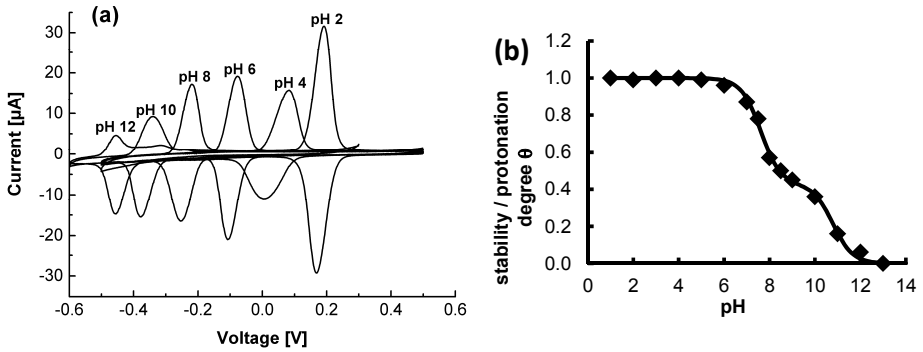

Figure 9. a) Cyclic voltammograms (10 mV s^{-1}) of PQQ immobilized on FWCNTs at different pH values (2-12) (Publication I). b) The relation of PQQ oxidation and reduction charge before and after 515 consecutive cyclic voltammograms (diamonds) and the deprotonation degree of a two pKa system (solid line, $pKa_1 = 7.6$ and $pKa_2 = 10.8$).

4.1.3 The role of carbon support

Metal nanoparticles are prone to agglomeration, so in order to use them as DMFC catalyst support materials are used to stabilize them. The support should provide anchoring places for the catalyst nanoparticles to grow and bind them well enough that they do not travel on the surface to agglomerate with other nanoparticles or detach completely. It should also be conductive for electron transfer, stable in the fuel cell conditions (corrosion resistive) and have large surface area to enable high catalyst loading and activity. SnO_2, TiN, TiB, ITO and tungsten oxides are used [93] but the largest interest and current use is concentrated on carbon-based support materials [94].

Carbon black has been the first choice for fuel cell catalysts supports due to its high surface area and affordable price. It is manufactured by pyrolysis of hydrocarbons like acetylene or oil fractions. It is partly crystalline and the crystallinity degree can be controlled by the process temperature. Due to the variations in production its properties can vary greatly: the specific surface area can be from 50 to 1500 $m^2\ g^{-1}$ with varied pore distribution and the average particle diameter between 15-40 nm [95]. Vulcan from Cabot Corporation, which is often used as a support, has specific surface area of 150 $m^2\ g^{-1}$ with a majority of pores in the range of 5-20 nm (mesopores) and particle sizes in tens of nm (Publication IV). Larger pores can be advantageous as they should be able to accommodate the catalyst particle, the ionomer and still have enough pore volume left for reactant and product transport (Chapter 5).

However, carbon materials are susceptible to carbon corrosion in fuel cells conditions. This is simply due to electrochemical carbon oxidation to CO_2 ($E^0 = 0.207$ V) in the potential range of the anode and the cathode and at operational DMFC temperatures

[96]. The problem is enhanced during fuel cell start-stop cycles and fuel starvation conditions, when part of the anode is covered by fuel and part is still covered by air or water. This situation can result in corrosion of the cathode of a H_2-PEMFC [97] and anode of a DMFC [98,99], which decreases the fuel cell performance and hydrophobicity of the CL. Moreover, the presence of Pt and Ru increases the oxidation rate [100]. It has been shown that carbon black is more prone to oxidation than graphitic carbon, *e.g.* CNTs [62] and CNFs [101], and therefore they have been studied as catalyst supports for fuel cells.

CNTs and CNFs also have other interesting properties like high electrical conductivity and high surface area [102]. The main structural difference between the CNTs and CNFs is graphene edge plane exposure: while CNTs are tubular structures showing mostly the basal plane and the edge plane only at tube ends, CNFs are stacked with individual graphene layers exposing the edge planes along the fiber growth axis with no inner cavity like inside of the inmost CNT. They also have different dimensions: the diameter of SWCNTs is from 0.4 to 2.5 nm, while MWCNTs can be 100 nm and their lengths range from a few μm to hundreds of μm. The CNFs are generally much thicker, up to 500 nm, while the length scale is the same. The FWCNTs used in Publications I, III and IV are 3-8 nm in diameter and 1 μm in length and the GNFs in Publications II and IV are commercial (Showa Denko) with 150 nm diameter and 10 μm length. Graphitization at high temperatures (2000°C) was used to increase the graphitic content of the CNFs and to improve their electrical conductivity and mechanical properties.

Although many of these alternative supports have been tested in DMFC [103-117], their long-term stability in DMFC conditions has not been studied widely though it is a significant reason for their research [33,118]. In light of this, Vulcan-, GNF- and FWCNT-PtRu were tested for a period of 3 days in a micro-DMFC anode in Publication IV. The chronoamperometric measurements at 0.2 V for these catalysts are presented in Figure 10A and the polarization curves before and after this measurement in Figure 10B. It is clear that the performance order of the catalyst supports is FWCNT > GNF > Vulcan. This can be partly due to the improved conductivity of the FWCNTs and GNFs when compared to Vulcan. Additionally, the PtRu catalyst particle size was the smallest for the fresh FWCNT-supported catalyst increasing its active area: diameters were 3.6 (Vulcan), 3.6 (GNF) and 2.8 nm (FWCNT). Part of the performance enhancement can be also due to the more open 3D structure of the CL that is considered in more detail in Chapter 5.3.2. Comparisons to previous studies with different carbon supports are difficult to make as Steigerwalt *et al.* [115] showed that with different types of CNFs, the DMFC performance could vary from 350 to 1100 mA cm^{-2} at 0.2 V and concluded that the performance order of the tested supports was CNF > PtRu black > SWCNT >

MWCNT. In contrast, Girishkumar *et al.* [116] measured maximum power densities of 4.0, 3.5 and 1.0 mW cm^{-2} for SWCNT from three different manufacturers in a free-breathing DMFC and indicated that the performance order of the supports was SWCNT > MWCNT > CNF > Vulcan. Steigerwalt *et al.* [115] had also wide variety of catalyst nanoparticle sizes from 4.8 to 8.6 nm on the different supports, while Girishkumar *et al.* [116] did not report the particle sizes unlike in Publication IV. Neither of these papers reported any details of the CL structure making DMFC analysis even harder. In the study by Santasalo-Aarnio *et al.* [33] resembling Publication IV in catalyst properties and measurements but done in a standard test DMFC instead of a micro-DMFC, the order was Vulcan > GNF > FWCNT. The possible reasons for the performance differences are discussed in Chapter 6.3. All in all, it is very difficult compare the catalytic activity of catalysts between different studies in DMFC because of the widely varying catalyst synthesis and resulting particles as well as the many ways of preparing MEAs and the parameters of the DMFC measurements. However, generally it can be stated that the different CNT and CNF supports can be used to improve DMFC anode performance when compared to Vulcan supports.

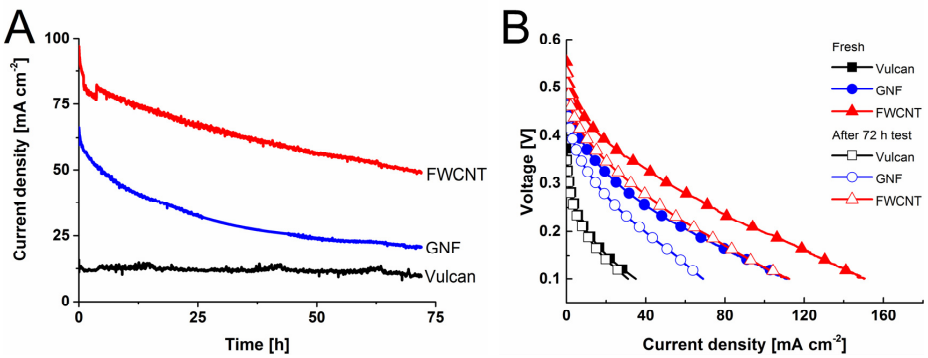

Figure 10. 72-hour chronoamperometric measurements at 0.2 V in Nafion-based micro-DMFC with PtRu supported by different carbon materials on the anode (A) and the polarization curves for each MEA before and after the chronoamperometric measurement (B). (Publication IV)

The stability of the FWCNT and GNF supports during and after the chronoamperometric measurement is not as good as the Vulcan support as seen from Figure 10, contradicting the idea that the alternative supports should be more resistant to DMFC conditions than Vulcan. However, the Vulcan supported catalyst particles agglomerated and grew in diameter to 5.5 nm while FWCNT- and GNF-supported particles did not show changes indicating that the FWCNTs and GNFs do protect the particles against agglomeration. A possible catalyst related reason for the different stabilities is that the Pt particle size does not influence the mass specific activity of methanol electro-oxidation in the range of 3.0 to 4.5 nm [119] explaining why Vulcan-supported catalyst shows stable performance. The poor stability of GNF-supported catalyst is due to the poor anchoring of the particles as the GNF type was tubular,

which has the lowest number of active edge sites thought to stabilize the catalyst particles [118,120]. Also, the CL structure changes so that the layer from Vulcan and GNF-supported catalyst lose secondary porosity, while FWCNT-supported remains unchanged (see Figure 17 in Chapter 5.3.2). Furthermore, the micro-DMFC GDL structure from Si nanograss (see Chapter 6.1.2) may not have been enough to handle the increased water production of the more active catalysts decreasing their performance due to increased water accumulation in the cathode. The long term durability of the GNF support was also studied in Publication II, where Nafion MEAs with an anode made from GNF-PtRu were subjected to 220 h chronopotentiometric measurements at 27 mA cm^{-2}. The voltage decay could be decreased by increasing the Nafion content of the anode from 30 wt% (124 μV h^{-1}) to 50 wt% (11 μV h^{-1}) and to 70 wt% (-124 μV h^{-1}) with the highest maximum power density achieved with 50 wt%. The decay rates are low or even positive at the higher Nafion contents but longer tests (2000 h [118]) have indicated that the overall decay rate is around 20 μV h^{-1}, which was 30% less than for commercial carbon black supported PtRu.

In conclusion, it can be said both FWCNTs and GNFs show promising properties for PtRu catalyst supports, but even though their DMFC performance is much higher than with Vulcan support it is not as stable. However, it could be shown that at least with GNFs the DMFC performance could be stabilized with the modification of the CL as the large secondary pores allowed the use of higher binding Nafion content, which resulted in stable performance over 220 h.

4.2 Oxygen reduction

4.2.1 Pt-based catalysis

Although Pt is hampered by the methanol crossover (Chapter 2.3) from the DMFC anode, it is generally used as the cathode catalyst due to its high activity towards ORR, good stability and excellent selectivity to the full 4 electron reduction to H_2O. The simplified model of the ORR in acid and alkaline is presented in Figure 11.

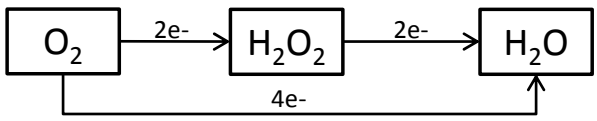

Figure 11. Simplified mechanism for ORR on Pt.

As with the MOR, the reaction starts with adsorption of O_2 to the Pt surface [121]. The direct reduction to H_2O proceeds via dissociation of the O_2 molecule:

$$O_{2_{ads}} \rightarrow O_{ads} + O_{ads} \quad \text{(xx)}$$
$$2O_{ads} + 2H^+ + 2e^- \rightarrow 2OH_{ads} \quad \text{(xxi)}$$
$$2OH_{ads} + 2H^+ + 2e^- \rightarrow 2H_2O \quad \text{(xxii)}$$

Hydrogen peroxide is generated if the O_2 molecule reacts without bond-breaking with water in a 2 electron reaction. It can then either desorb and diffuse away or react with water following a consecutive 2 electron reduction pathway:

$$O_{2_{ads}} + 2H^+ + 2e^- \rightarrow H_2O_{2_{ads}} \quad \text{(xxiii)}$$
$$H_2O_{2_{ads}} + 2H^+ + 2e^- \rightarrow 2H_2O \quad \text{(xxiv)}$$
$$H_2O_{2_{ads}} \rightarrow H_2O_2 \quad \text{(xxv)}$$

In alkaline conditions, the reaction is similar except O_2 reacts with water instead of protons [122,123]. For the direct pathway:

$$O_{2_{ads}} \rightarrow O_{ads} + O_{ads} \quad \text{(xxvi)}$$
$$2O_{ads} + 2H_2O + 2e^- \rightarrow 2OH_{ads} + 2OH^- \quad \text{(xxvii)}$$
$$2OH_{ads} + 2e^- \rightarrow 2OH^- \quad \text{(xxviii)}$$

For the H_2O_2 producing pathway:

$$O_{2_{ads}} + H_2O + 2e^- \rightarrow HO_{2\,ads}^- + OH^- \quad \text{(xxix)}$$
$$HO_{2\,ads}^- + H_2O + 2e^- \rightarrow 3OH^- \quad \text{(xxx)}$$
$$HO_{2\,ads}^- \rightarrow HO_2^- \quad \text{(xxxi)}$$

The reaction on carbon supported Pt is practically H_2O specific in acid conditions [124], although the presence of Nafion can slightly increase H_2O_2 production to a percent most likely as a result of sulfonate interactions [125]. In alkali, a few percent of H_2O_2 can also be produced [126,127]. H_2O_2 is a strong oxidizer and can degrade the Nafion membrane in the fuel cell through radical formation [128,129]. In addition, as O_2 molecules do not use all of their electron acceptor capacity, the current density will decrease. This in combination with the high price of Pt, its susceptibility to methanol crossover and the formation of Pt oxides in fuel cell conditions [130] are motivating factors for the development of catalysts for ORR by either modifying Pt [131] or by developing new, non-precious metal catalysts (Publication III) [132].

4.2.2 Nitrogen-modified carbon catalysts

Carbon materials with nitrogen-doping were first shown to have ORR activity already in 1960s in the form of phtalocyanines complexed with non-precious metals like cobalt or iron [133]. Later, it was realized that ORR active catalysts could be derived simply by the combined heat-treatment of a metal precursor, a carbon material and a nitrogen source [134]. In recent years, these catalysts have reached activity and stability close to Pt at low and medium current densities in H_2-PEMFCs [135,136].

However, in 2009 Gong *et al.* [137] published a paper showing that vertically aligned CNTs with N-doping could catalyze ORR as well as Pt in alkaline solution without any metal residues from the synthesis. The catalytic activity has been attributed to the positive charge on carbons caused by the more electronegative nitrogen [137], the enhanced H_2O_2 decomposition rate on N-doped carbon [138] and the large amount of edge sites in N-doped graphitic carbon [139], however the exact mechanism of reaction is not yet clear. Since then a great variety of graphitic material has been N-doped with various techniques resulting in good ORR activity in alkaline solutions and mediocre activity in acidic solutions [140-143]. Examples of N-doped graphitic carbon active for ORR include graphene [144-146], CNTs [147-149], carbon nanofibers (CNF) [138,150], mesoporous carbon [141,151] and carbon spheres [152,153] among others. There have been speculations that the catalytic activity is a result of metal residues from carbon material synthesis as described in the previous paragraph due to the difficulty of removing all the metal, but recently N-doped carbon materials synthesized without metal catalyst have been shown to be as active [141,151,152]. Moreover, cyanide, which is reported to poison a Fe-C-N catalyst [154], had no effect on the ORR activity of an N-doped carbon [155].

Even though the research of these N-doped carbon catalysts is intensive, actual fuel cell testing is still lacking. There have been some studies which utilized these catalysts at the cathodes of acidic H_2-PEMFCs [156-160] and a DMFC [161], but there are only a few studies where alkaline anion-exchange membrane fuel cells have been used (with H_2 [162,163] and methanol (Publication III) [164]). As these catalysts are expected to work better in alkaline conditions, it is not surprising that improved performance when compared to Pt has been achieved with the alkaline fuel cells (Publication III) [162,164], while the performance of Pt-free catalysts in acidic fuel cells is lower than that of Pt.

The objective in Publication III was to synthesize N-doped carbon material and compare it to commercial Pt catalyst in an alkaline DMFC cathode with both air and

oxygen as the oxidant, which has not been previously investigated in this system and with these catalysts. The only previous study with an N-doped material at an alkaline DMFC cathode was by Sun *et al.* [164], where the focus was on synthesis of doped carbon from commercially available carbon blacks and the catalyst was co-doped with fluorine. In Publication III, a more conductive and robust material, FWCNTs (see Chapter 4.1.2), was selected and the doping method was pyrolysis of a polyaniline layer adsorbed on the FWCNT surface [34]. This formed a thin N-doped layer on top of the FWCNTs (N-FWCNT) with minimum defects in the CNT walls thus maintaining their electrical and mechanical properties. The nitrogen content was low, 0.56 at%, but the nitrogen was primarily located in pyridinic and graphitic sites, which are thought to be the most reactive [165]. Its ORR activity in RDE measurements was close to that of Pt and the selectivity to 4 electron reduction to H_2O high [34]. The performance of the alkaline DMFCs constructed from Fumatech FAA3 membrane and ionomer with the N-FWCNT and the commercial Pt catalyst cathodes are presented in Figure 12.

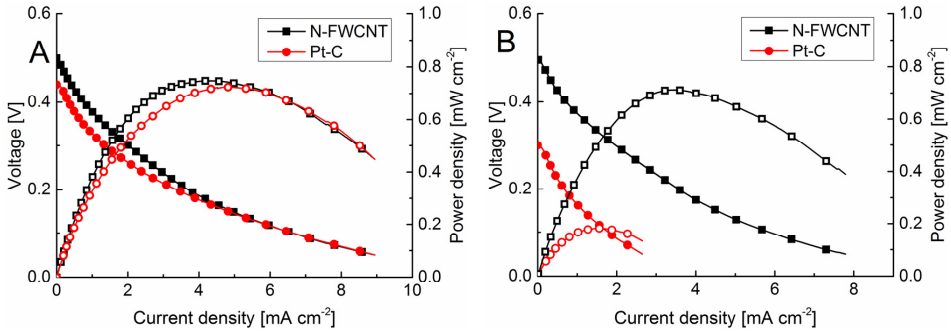

Figure 12. The alkaline DMFC performance of the N-FWCNT cathode (2.3 $mg_{(N\text{-}FWCNT)}$ cm^{-2}) and Pt/C cathode (0.5 $mg_{(Pt)}$ cm^{-2}). A) O_2, B) air as the oxidant. The full symbols refer to voltage curves and open symbols to power curves. The membrane and ionomer used were FAA3 from Fumatech (Publication III).

With pure O_2, the performance of the N-FWCNT catalyst is slightly better than Pt (Figure 12A): the maximum power density obtained is 0.78 mW cm^{-2} compared to 0.72 mW cm^{-2} with Pt indicating an 8% increase. The difference is in the same range as Sun *et al.* [164] measured with their catalyst in alkaline DMFC (15% increase). The absolute power densities are lower than those achieved by Sun *et al.* [164] but that is explained by the fact that they added KOH to the methanol solution to make it basic and enhance the DMFC performance [10]. Furthermore, their measurement temperature was higher (60°C vs 50°C) and the membrane material allowed hot-pressing of the MEA, both of which contribute to the better performance. There are no other DMFC tests done with FAA3 to compare the results to but a test with the previous membrane version FAA2 at 30°C showed a maximum power density of 0.3 mW cm^{-2} [166] indicating that FAA3 works better. The higher OCV with N-FWCNTs is indicative of excellent methanol tolerance, which was also seen in the RDE experiments [34]. The stability of the N-

FWCNTs were reasonable with a current decay rate 43 μA cm^{-2} h^{-1}, which corresponded to a decay rate of 2.2% h^{-1} relative to the starting current density of 2 mA cm^{-2} at 0.2 V. The instability could be caused by the detachment of the thin N-doped layer but comparison of X-ray photoelectron spectroscopy (XPS) and TEM images taken before and after the measurement was inconclusive due to the ionomer interfering with the nitrogen XPS signals and the visual imaging of the N-FWCNTs.

When synthetic air (80% N_2, 20 % O_2) was switched to the cathode, a dramatic and previously undocumented drop in Pt performance was observed, while N-FWCNT sustained high performance: the maximum power density was reduced by only 6% for the N-FWCNTs and 75% for the Pt. Additionally, the OCV with the Pt dropped significantly from 0.44 to 0.30 V, while the OCV with N-FWCNT remained at 0.50 V. This indicates that the decrease in O_2 concentration at the cathode allows methanol to significantly disrupt the cathode performance. This is likely due to the fact that methanol at the cathode oxidizes and consumes O_2 leaving the area around catalyst sites even more depleted of O_2 than the 80% decrease in partial pressure from pure O_2 to air. In contrast as N-FWCNTs are inactive toward MOR, methanol simply diffuses out of the CL. However, the drop in DMFC maximum power density when pure O_2 is switched to air is usually between 10 and 50% with Nafion and Pt depending on the conditions [20,167,168]. At the same temperature (50°C) and methanol concentration (1 M), Scott *et al.* [5] reported a 30% performance decrease for an alkaline DMFC using Pt. On the other hand, they used a different membrane (ADP-Morgane®) and Nafion as the CL binder, which affects the behavior of the DMFC. The properties of FAA3 membrane should be studied more extensively to determine if *e.g.* an unexpectedly large methanol crossover is the reason for the poor performance with Pt and air. For FAA2 methanol permeability was 0.5 cm^2 s^{-1} which is 1/6 of the permeability through Nafion and in the same range as other alkaline membranes [169]. The reason for the small 6% performance decrease with N-FWCNTs may also be due to a very open CL structure compared to commercial carbon supported Pt (see Figure 18 for SEM images). These large pores facilitate the mass transfer enabling better availability of O_2 through the whole CL and the removal of water and methanol from crossover.

In conclusion, in Publication III it was shown that noble metal free N-FWCNTs with very low nitrogen content are suitable for replacing Pt at the cathode of an alkaline DMFC as they perform as well as Pt when O_2 is the oxidant and 4 times better with air due to their methanol tolerance and open CL structure. It was the first time N-doped carbon materials were tested in an alkaline DMFC with air as the oxidant and it will be interesting to see if the same phenomenon can be repeated on other alkaline membrane materials.

5. Fuel cell electrode structure

5.1 3-phase boundary

The most important part of a fuel cell is the CL and the interfaces within. Three different pathways are required for a catalyst particle to be active: a porous channel for reactant delivery, an electron conducting structure to lead the electrons to the external circuit and an ion-conducting pathway for the protons or hydroxide-ions to reach and travel through the membrane. Even if one of these phases is missing or is not continuously connected to the flow field, current collector or membrane in the proximity of the catalyst particle, the electrochemical reaction cannot proceed at that site (Figure 13). This region is often called the three-phase boundary and it is a common feature in most fuel cell types. If the electrolyte is a liquid, like in a molten-carbonate fuel cell or alkaline fuel cell, the electrode fabrication is less problematic since the electrolyte will penetrate the electrode and conduct ions from any available active sites, while for fuel cells employing a solid electrolyte, like solid-oxide fuel cells and PEMFCs including DMFCs, the fabrication has to be more controlled as the electrolyte is immobile.

Figure 13. Schematics of the CL structure and the 3-phase boundary with solid electrolyte. Green: the membrane and the ionomer, black: carbon, grey: catalyst particle. Particles marked with red are active due to simultaneous access to carbon, ionomer and pores.

It is also worth noting that the form of the fuel and the oxidant is also relevant to the 3-layer boundary and CL design. For example, in an acidic H_2-PEMFC, hydrogen is fed to the anode and the protons produced travel through the membranes simplifying the mass-transfer in the CL. At a DMFC anode, aqueous methanol solution is usually used and gaseous CO_2 is produced and removed from the CL. These differences make it difficult to utilize results from one type of a fuel cell in another type of a fuel cell. Accordingly, this chapter will mostly discuss fuel cell performance in DMFCs as it is the primary focus of the thesis in respect of catalyst studies but relevant results on CL structure (porosity, catalyst utilization) in a H_2-PEMFC MEAs are also discussed as the materials are the same in the two systems.

5.2 Membrane-electrode assembly fabrication history

Historically, fuel cell electrodes were made with Teflon or other hydrophobic plastic materials as the binder. This enabled good pathways for the gaseous reactants to reach the catalyst particles but left most of the catalyst inactive since there was no ionomer to transport the ions to the membrane. In practice, only the catalyst particles very close to the membrane were active and high Pt contents at H_2-PEMFCs cathode were necessary to reach sufficient power levels (4.0 mg cm^{-2}) [170]. When the role of the ionomer was realized, it was first used to cover the Teflon-bound electrodes with a Nafion dispersion, which allowed a deeper layer of the catalyst to be active and reduced the required catalyst amounts to 0.4 mg cm^{-2} [171]. The final breakthrough in electrode preparation was the development of thin film techniques, where the Teflon binder was replaced by Nafion binder. The CL is prepared from an "ink", which contains the catalyst mixed with ionomer dispersion and solvents that is then sprayed, brushed or printed on the GDL, membrane [36] or plastic film for decal transfer [172]. This means that the whole CL is impregnated with the ionomer and much higher catalyst utilization can be reached reducing the catalyst loadings further to 0.1 mg cm^{-2} [36]. As the lowered amount of catalyst enables CLs that can be less than 10 μm thick, this method is commonly known as the "thin film method". CLs fabricated this way consist only of useful parts for 3-phase boundary: the catalyst, the electron conductor, the ion conductor and pores. The pores in the thin film layer can be defined as primary pores, which exist between catalyst particles (0.02-0.04 μm), and secondary pores, which exist between the agglomerates of catalyst particles and the ionomer (0.04 μm to micrometers) [173].

Other fabrications methods for MEAs [174,175] have been developed recently (*e.g.* electrodeposition [176], sputter deposition [177], pulsed laser deposition [178], dry spray [179], stencil [180], layer-by-layer [181]) but as the thin-film method is the state-

of-the-art way of fabricating experimental DMFC MEAs and all the MEAs used in this thesis are made by this method, the other techniques are not analyzed here. The interested reader is directed to the references quoted above.

5.3 Fabrication of catalyst layers with thin film methods

5.3.1 Ionomer content

The most direct method to change the CL properties is to change the amount of its constituents. In the most common case there are only two constituents, the catalyst and the ionomer and the amount of ionomer can be addressed alone as the amount of catalyst changes reciprocally. The most common way to refer to the ionomer content is to report its weight percentage as part of the whole CL dry weight and this convention is also used in this thesis.

As can be seen from Figure 14, the fuel cell performance is highest at certain ionomer content (in this case 40 wt% of alkaline FAA3 ionomer) and decreases as the ionomer content approaches 0 or 100 wt%. This is due to the changes in the 3-phase boundary. At very low ionomer content, the CL is highly porous and thin, making the mass-transfer fast; however the ionomer conducting pathways are not penetrating the whole layer thus reducing the catalyst utilization. When the ionomer content is very high, the ionomer blocks mass transfer through pores and can isolate catalyst particles from the electrically conducting pathways again reducing the catalyst utilization. Therefore, the optimum performance is found at some intermediate ionomer content value. In some special circumstances like in the case of unsupported PtRu catalyst with high proton conductive hydrous Ru-oxide content, it is possible to have an optimum at 0 wt% ionomer [182].

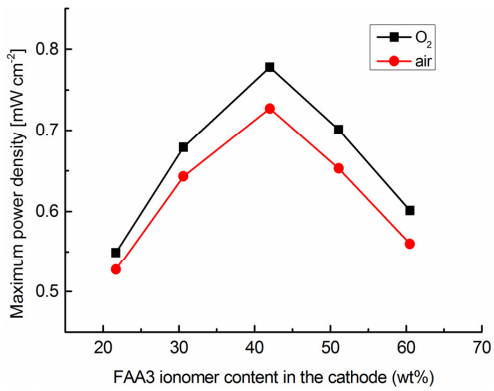

Figure 14. The maximum power density of an alkaline DMFC as the function of ionomer content in the cathode CL containing N-doped FWCNTs. (Publication III).

The exact value of the optimum ionomer content depends on the catalyst and ionomer type as well as MEA preparation method, the fuel cell type and operating conditions [183,184]. For example, when using commercial carbon black supported PtRu, the optimum Nafion content for a DMFC anode has been determined to be between 25 and 40 wt% [180,183,185,186], while for GNFs the optimum is around 50 wt% (Publication II) and for MWCNTs 62 wt% [104]. This is most likely due to the fact that the long and thin CNF and CNTs form bundles and tangle with each other leaving a lot of empty space in the CL that has to be filled partially with the ionomer. For the DMFC cathode, the optimum has been measured to be between 20 and 35 wt% of Nafion for carbon black supported catalyst, while in an alkaline DMFC using N-doped FWCNTs, the optimum was 40 wt% (Publication III). If unsupported catalyst is used, the optimum is between 10 and 20 wt% [182,184,187,188] as the thinner CL requires less ionomer to saturate. These examples underline the importance of the optimization of the CLs for the specific testing conditions as an unoptimized structure can decrease the performance of a DMFC even by half (Publication II and III) [180,184,188] and this could make *e.g.* new catalysts appear less suitable for fuel cell applications.

The change in the CL structure with different ionomer contents can be easily seen from SEM images. In Figure 15, DMFC anodes based on PtRu-GNF with Nafion contents of 30, 50 and 70 wt% are presented (Publication II). It is clear that the CL becomes denser and less porous as the Nafion content increases. The specific surface area of the CLs was measured by 1-point BET N_2 desorption directly from MEAs containing one electrode and was 0.8, 0.7 and 0.3 $m^2\ g^{-1}$ for 30, 50 and 70 wt% of Nafion, respectively, confirming the visual observations from SEM. The specific surface area of a pure Nafion membrane sample was 0.3 $m^2\ g^{-1}$ indicating that with 70 wt% of Nafion the CL starts to resemble a membrane. In this case, the conductivity reached a maximum with a 50 wt% Nafion content, which was attributed to the large volume of voids present with 30 wt% Nafion and the improved dispersion of GNFs in higher Nafion contents [189,190]. However, it is important to realize that increasing Nafion content increases the ionic conductivity of the CL and decreases its electrical conductivity [180,188,191].

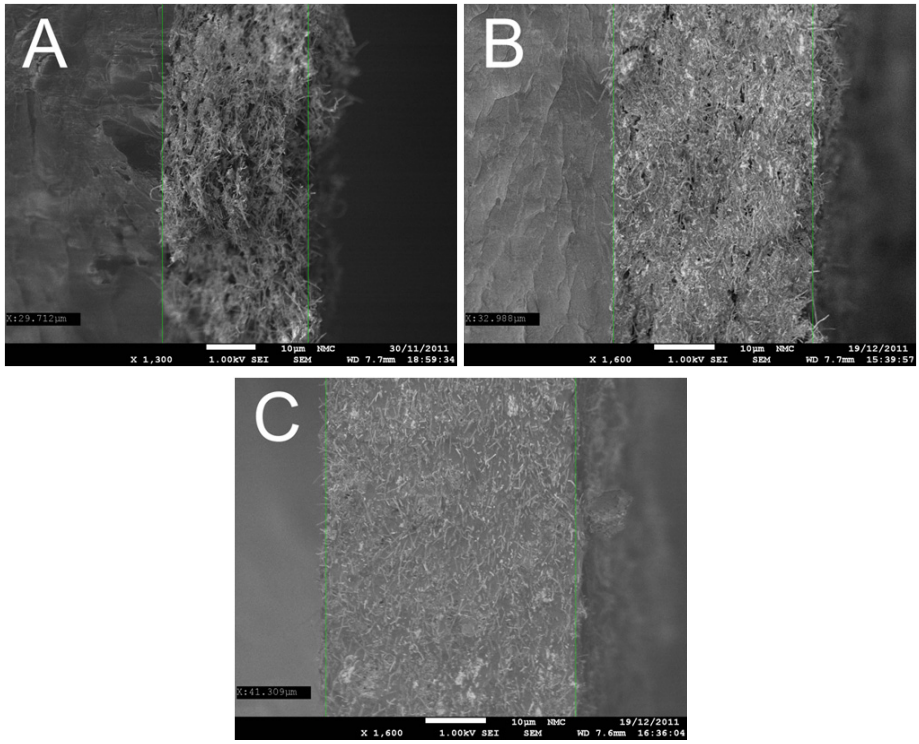

Figure 15. GNF-PtRu based DMFC anodes with different Nafion contents. A) 30, B) 50 and C) 70 wt% of Nafion. (Publication II)

Even though the resistivity and the thickness of the CL increases as the ionomer content increases, the contact resistance between the CL and the membrane decreases as the CL becomes more membrane-like and dense. Thus, the resistance of the whole MEA reaches a minimum at a certain ionomer content value depending on the CL structure (Publication III) [185,186,188,192].

The MEA durability can also improve with the ionomer content. During 220 h chronopotentiometric measurements (Figure 16) it was seen that with 30 wt% Nafion the fuel cell performance decreased the most while with 70 wt% Nafion the performance improved as the higher ionomer content makes the CL more resilient to degradation. To the best of the author's knowledge this was the first study in which DMFC stability as a function of the ionomer content was investigated.

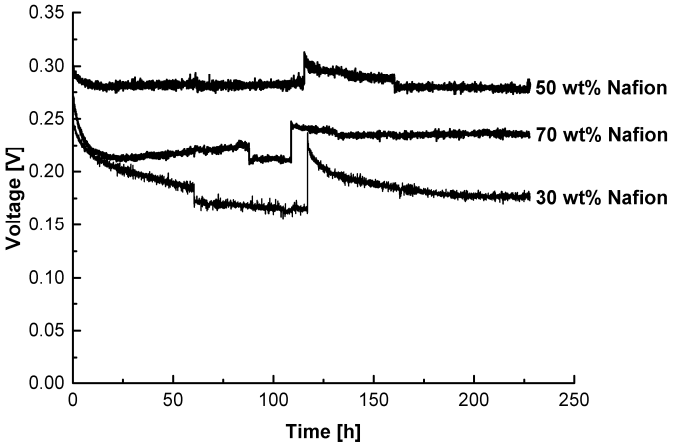

Figure 16. Chronopotentiometric measurements (27 mA cm^{-2}) of DMFCs with GNF-PtRu anodes containing different amounts of Nafion ionomer. (Publication II)

5.3.2 Carbon supports

A large part of the total volume of the CL is taken by a carbon support of the metal catalyst or the carbon-based catalyst and the type of the carbon can have large impact on the CL structure. However, this has not been widely investigated in the literature (Publications II, III and IV) [33,107,117] as most studies of different catalyst supports in a DMFC only report the performance [103-106,108-116]. In Publication IV, three PtRu catalysts with different supports (carbon black, GNF, FWCNT) were synthesized and their performance and structure as Nafion-based micro-DMFC anode catalyst were examined. In Figure 17, the SEM micrographs of the anode CLs are presented and it is immediately obvious that the CLs have very different secondary structures. With carbon black (Figure 17A), the CL appears quite dense and uniform, there are no large, deeply penetrating cracks and the secondary pores are small (<<1 μm). With GNF (Figure 17B), the CL has large secondary pores with the individual GNF protruding randomly out of the CL. This structure resembles closely the one seen in Figure 15A, which is made with the same materials at the same ratio. With FWCNT support (Figure 17C), the CL has little porosity visible but it is divided into relatively large (2-4 μm) agglomerates with cracks between them. However, the metal loadings on the supports and in the CLs are similar in each case as is the CL thickness, so the total pore volume in the layers should be approximately same.

Both the FWCNT- and GNF-supported PtRu showed higher performance than the Vulcan-supported in the DMFC indicating that the CL structure with large secondary pores is beneficial for DMFC performance (Figure 10) most likely as a result of better mass-transfer through the relatively thick layer (~30 μm). The performance of the GNF

and FWCNT can also be improved by optimizing the ionomer structure. In Publication II, the optimum Nafion content of a GNF-based DMFC anode is determined to be 50%, while 30 wt% of Nafion was used in Publication IV. If this optimized value would have been used, the GNF-supported catalyst could have performed 30% better and be almost as good as the FWCNT-supported and as stable as the Vulcan-supported. These results indicate that the activity and stability of the different catalysts can easily be affected by the CL structure and that different catalysts should only be compared at optimized conditions for each one, otherwise the results may look unfavorable for the new, unoptimized catalysts. However, this is practically never taken into account when new catalyst materials are tested but the same conditions are used for all the catalysts.

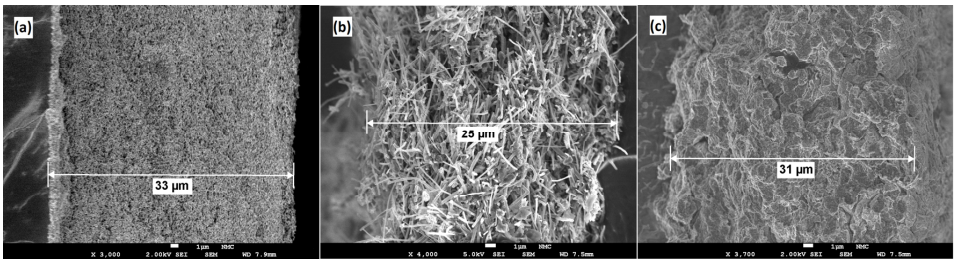

Figure 17. SEM micrographs of DMFC anodes with Nafion and PtRu catalyst supported on various carbons. Supports: A) Carbon black (Vulcan), B) GNF, C) FWCNT. (Publication IV)

If the FWCNT are doped with nitrogen, the agglomerated structure is clearer than in the undoped case. In Figure 18A, a high magnification SEM image of an N-FWCNT cathode with alkaline FAA3 ionomer is shown and the secondary pores are clearly visible with agglomerates (1-3 µm) of ionomer and N-FWCNT composite. On the other hand, the CL with commercial high-surface area carbon supported Pt and FAA3 in Figure 18B shows a similar structure to the CL with carbon black supported PtRu and Nafion in Figure 17A. The catalyst and ionomer agglomeration can be explained by the CNT-Nafion interaction [189,190,193]. When CNTs are dispersed into a polar solvent containing Nafion ionomer, there is a hydrophobic interaction between the fluorinated carbon chain of Nafion and the surface of the CNT. Long Nafion polymer chains wrap around the individual CNTs in multi-helical way disrupting the strong van der Waals – interactions between them that would otherwise cause precipitation [193]. However, the CNTs bundle near metallic catalyst particles due to their easily charged nature [189]. The combination of these two effects may cause the single Nafion-CNT agglomerates coalesce during the CL preparation forming the structure seen in Figure 17C. As nitrogen is more electronegative than carbon it causes charge localized separation in the FWCNTs [137], therefore the N-FWCNTs in Figure 18A may promote agglomeration with the charged ionomer causing the more clearly separated agglomerates. Also, the charge of the anion-exchange ionomer FAA3 is opposite to the

cation-exchanging Nafion and its molecular structure different, which can also explain the observed differences in the CLs.

In the case of the GNFs, increasing the Nafion amount stabilized the ink (Publication II), so it is likely that Nafion can also wrap around the individual fibers but as the fibers are 30 times thicker, the Nafion layer only covers the fibers and does not combine them in agglomerates. On the contrary, Pt/carbon black+Nafion dispersion in an isopropanol-water mixture has been shown to contain multiple particle sizes and geometries of agglomerated carbon in the range 60-200 nm [194] that can produce a structure with small secondary pores and continuous layer. Similar results were obtained from pure carbon black (Vulcan) samples [195] indicating that adding Nafion binds carbon black particles together unlike with pure CNTs [190].

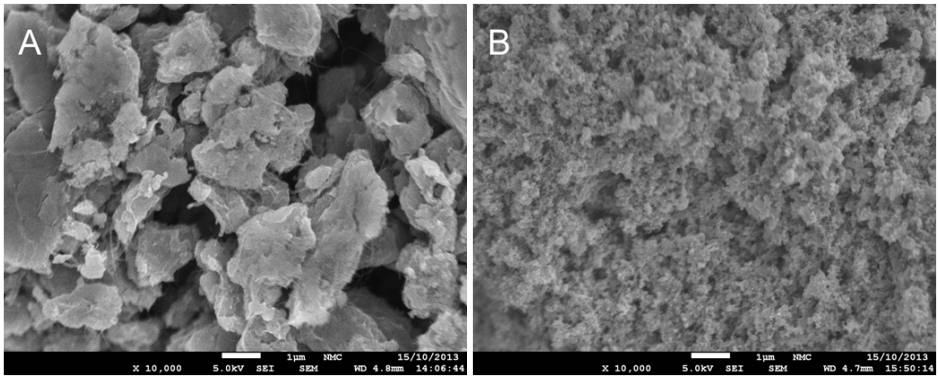

Figure 18. SEM micrographs of DMFC cathodes with FAA3 as the ionomer (30 wt%). A) N-doped FWCNTs, B) commercial Pt supported on high-surface area carbon (Alfa Aesar). (Publication III)

The carbon support has also an effect on the wetting properties of the CL. The contact angle between water and the CL surface was measured for each MEA in Figure 17 (Publication IV). The unused carbon black and FWCNT MEAs showed similar hydrophobic contact angles of ~155°, while the uneven nature of the GNF MEA edge caused the contact angle to rise to 164°. This increased hydrophobicity can be beneficial for gas removal from the CL.

5.3.3 Fabrication techniques

Ink application methods

The way the catalyst ink is applied to a substrate to form the CL has some influence on its structure. Spraying by air-brush is the most common way of fabricating the CL and it is used throughout this thesis but some alternatives exist.

Screen-printing is a method where the ink is forced through a tight mesh by a squeegee to the substrate. Due to some agglomeration in the ink and uneven drying during the spraying process, the screen-printed CL shows a more uniform and compact structure [196-199]. At a same commercial catalyst loading (0.15-0.60 mg cm^{-2}), the sprayed CL are 10-20 μm thicker and have larger secondary pores than the comparable screen printed CL [196,198]. Based on these results, a new hybrid method for MEA preparation was developed, where the diffusion layer is sprayed to enable a more efficient distribution of reactants and product removal and the CL is printed on the diffusion layer for better contact between the ionomer and the catalyst [197]. Doctor blade application resembles screen-printing but the thickness of the film is controlled by separation of the blade and the substrate and there is no mesh [200]. Commercial inkjet printing has also been used with inks of finely tuned viscosity and surface tension to produce CLs [201,202]. Due to the very small volumes of ink deposited at a time, the catalyst loading can be accurately controlled even at low concentrations (<0.05 mg cm^{-2}). Screen-printing was tried during the work in this thesis for fabricating CLs of better reproducibility but printing of sufficiently high catalyst loading demanded many print runs and more ink than spraying, so it was not deemed to be suitable for use with these expensive catalysts.

In electrospraying, a high voltage (up to 4 kV) is applied between a capillary, where the catalyst ink flows, and a carbon substrate, where the CL is formed. The highly charged ink will break down to small droplets to form a mist that is attracted to the oppositely charged carbon substrate. With this technique, a more uniform CL structure with smaller pores than possible with air-spraying or by the impregnation method was achieved [203]. The CL structure was further improved by a hybrid technique, where air flow is directed through the electrospray nozzle [204]. Due to the complicated nature of the method and the possible difficulties with agglomerated inks from GNFs and FWCNTs, this method was not adopted for MEA fabrication in this thesis.

Manual painting of carbon supported catalysts with a brush is also sometimes utilized but should be avoided as the resulting CL layer is 4 times more uneven and 3 times less reproducible compared to spraying [205]. Since the ink may remain on the brush for a significant time and be partially dry before it is transferred to the painting substrate, the agglomeration of the particles is also considerable. However, Mao *et al.* [206] discovered that a brushed CL of PtRu black CL shows more secondary pores than a sprayed CL and recorded higher DMFC performance from the MEAs prepared by brushing. On the other hand, their cathode was made of carbon supported Pt, where the spraying method resulted in higher secondary porosity and cathode performance. It

seems that brushing can be beneficial for the dense CLs containing unsupported Pt or PtRu, which were not used in this thesis.

Ink application substrates

When Wilson and Gottesfeld introduced the thin film method, they specified two different methods to construct the MEA. In the decal method [172], the catalyst ink is spread on a Teflon decal (other decal materials can also be used [207]), dried and the resulting CL is hot-pressed against a membrane to transfer and intimately bind them together. In the direct coating method [36], the ink is applied to the membrane in the first place, whilst a third option is to apply the ink on the GDL, which is then pressed against the membrane. It has been shown that the best DMFC performance is achieved by the direct membrane coating method [207-210], while applying the coating to the GDL has produced the lowest performance [211,212]. This is likely due to the more intimate contact between the CL and the membrane as the ionomer in the CL can connect with the membrane as it rearranges during the drying process. Further hot-pressing makes this contact better. In the decal method, the CL is first formed and only then brought to contact with the membrane through hot-pressing. This forms a good contact as the CL is pressed against and bound to the membrane. In the coated GDL case, the CL may as well be pressed in to the soft carbon diffusion layer instead of the membrane making the contact between them less intimate. In addition, the GDL structure can also suffer during the hot-pressing process [213,214].

You *et al.* [207] showed that compared to the direct membrane coating, the CLs formed with the decal method are thinner but also less porous. This appeared to be more important in the case of the cathode as the ORR was more hindered according to impedance measurements while there was no difference in the anode performance. Reshetenko *et al.* [209] observed different secondary structures of CLs when coated on the membrane and GDL, while the microscopic structure was the same. It seems that the web-like secondary structure of the microporous carbon layer of the GDL continued to the CL, which resulted in CO_2 flooding of the GDL-CL at high current densities. The directly to membrane coated CL had smaller secondary pores, which facilitated the CO_2 removal and improved the DMFC performance. In light of this, direct membrane coating was used with Nafion-based MEAs in this thesis (Publications II and IV). For the alkaline FAA3-based MEA in Publication III, direct coating could not be used as the membrane dissolved in the ionomer ink. Decal-transfer method was tried but the CL could not be transferred reliably from the plastic substrate to membrane in limited temperature range of the membrane (<80°C). Finally, the ink was painted on a carbon cloth with microporous carbon layer.

Hot-pressing

Hot-pressing is used to bond the CL and the membrane together tightly. The method is related to the glass transition temperature of Nafion (around 120°C in ambient conditions) at which Nafion becomes softer and allows the fusing of the CL and the membrane [215,216]. It involves placing the MEA components between heatad plates that are pressed together at certain pressure for a period of time. Optimum values for the temperature, pressure and time for the hot-pressing are strongly dependent on the desired MEA structure. The following chapter describes only the results for Nafion as the alkaline membrane FAA3 was not subjected to hot-pressing as it loses its integrity when temperature and pressure are applied [37].

For the CL coated directly on membranes, the use of hot-pressing was first reported to be unnecessary for improved performance of a H_2-PEMFC [36]. However, Chen *et al.* [217] studied the hot-press parameters and the CL structure more closely for DMFCs. Their results showed that hot-pressing at higher pressure (100 kg cm^{-2}) decreased the thickness of the cathode and anode CL effectively reducing their porosity, which translated to a 50% smaller Pt utilization compared to a MEA hot-pressed at 5 kg cm^{-2}. The hot-pressing was also found to be critical for long-term H_2-PEMFC performance with non-pressed MEA degrading twice as fast as a pressed one [218]. Yazdanpur *et al.* [210] looked at the hot-pressing conditions for a H_2-PEMFC MEA employing a MWCNT-supported catalyst. Performance-wise the results agreed with Chen *et al.* [217] showing that decreasing the pressure from 105 to 55 kg cm^{-2} increased the power output. The press time and temperature were also examined and it was concluded that hot-pressing should be done for a maximum of 5 min or at 130°C. Accordingly, the MEAs fabricated in Publications II and IV were hot-pressed with 50 kg cm^{-2} (50 bars) at 130°C for 2 min. If hotter temperatures are needed, Nafion can be converted to Na^+ or tetrabutylammonium (TBA^+) in corresponding salt solution, which increases the heat tolerance of Nafion up to 200°C [219,220]. This is especially useful for the decal transfer method as the CL has to be transferred and attached completely to the membrane, which may require higher temperatures to succeed.

For the catalyst coated GDLs, several studies involving all the parameters have been done [214,216,221,222]. Generally, it can be said that high pressure (>100 kg cm^{-2}) can destroy the GDL and CL structure and that the temperature range is similar to membrane coated MEAs as the type of membrane and the ionomer are the temperature limiting factors.

5.3.4 Other methods to influence the catalyst layer

There are several other ways to influence the CL structure and improve the DMFC performance in the literature. These methods have not been used in this thesis as the object was to study the influence of ionomer content and catalyst support as simply as possible without other parameters influencing the measurements. A short review of alternative methods is given here.

Catalyst ink solvents

Catalyst ink solvents with a suitably low dielectric constant ($3 < \varepsilon < 10$) can be used to form micelles from perfluorosulfonate ionomers like Nafion [173,223], which in turn easily adsorb on catalyst particles making the ionomer network extensive and well connected. Nafion in solution form (solvent $\varepsilon > 10$) can penetrate some pores and block the catalyst particles in them from reactants [224]. Generally, it can be said that catalyst ink solvents with dielectric a constant $3 < \varepsilon < 10$ results in the best performance and large electrochemically active area. However, it should be noted that the use of solvents with too high boiling point can results in solvent residues that block pores in the CL [225]. In practice, Nafion is not recommended to be heated above 140 °C and the alkaline FAA3 to over 80°C, so the ideal solvents should have boiling point close to these values. Another important factor is that the resulting ink should be easy to spread to form the CL, so the solvent viscosity and ability to form a stable dispersion of the catalyst should be also taken into account.

Pore formers

Pore formers (PF) are solid or liquid substances that can be included in the catalyst ink and subsequently dissolved (*e.g.* $MgSO_4$ [207], Li_2CO_3 [226], SiO_2 [227]) or decomposed at elevated temperatures (*e.g.* $(NH_4)_2CO_3$ or NH_4HCO_3 [228,229], $(NH_4)_2C_2O_4$ [230]) so that pores or voids of similar size will be left in their place effectively increasing the porosity of the CL and improving its mass transfer properties. The influence of the PF particle size (SiO_2 spheres of 18, 42 and 500 nm diameters) was systematically studied by Lee *et al.* [227] who showed that even though the largest particles increased the total pore volume the least, they resulted in the best performance in DMFC indicating that larger pores are the most beneficial for mass transfer in the CL. When gaseous H_2O is present as in the cathode, this can be explained by the fact that liquids condensate more easily in small pores, thus blocking the mass transfer of gases [231]. For decomposable PFs, larger pores can be made by high decomposition temperatures resulting in rapid reaction and large pores (> 1 μm)

[232]. The optimum PF content for DMFC performance is 20-50 wt% depending on the PF [207,227,228,233,234] as the volume fraction of Nafion is reduced decreasing its effective conductivity [191], so a similar balance between the reactant and products transfer and conductivity is found. A too high PF content can also both decrease the stability of the CL and its adhesion to the membrane [235].

Additives

Both carbon black and vapor grown CNF has been added to catalyst inks to improve the porosity of the CL both at the DMFC cathode and anode, respectively. In the case of the cathode, improved performance compared to Pt black CLs were achieved and the difference increased as the DMFC operation mode was changed from pure O_2 to air and finally to a freely breathing cathode indicating improved O_2 mass-transfer [236]. In the case of the anode, the clearest improvements were seen at high current density and at low temperature also indicating enhanced mass transfer [237]. Additionally PTFE has been added to catalyst inks to increase the volume of secondary pores and hydrophobicity of the CL but it also competes harmfully with Nafion in contacting the catalyst particles, so its use is not recommended [238].

Boiling

After the MEA is fabricated the porosity of the CL can be increased by steaming or boiling it [239,240]. The total pore volume of the MEA increased 30-40 fold after 2 hour boiling and subsequent drying most likely due to Nafion expansion and contraction at different humidity levels.

6. Micro fuel cells

A micro fuel cell (MFC) is a fuel cell which has parts that are fabricated with micromachining. In practice, this means that the flow field, the electrolyte medium, GDL and/or the current collector are microfabricated. In this thesis, H_2-MFCs (PEMFCs with H_2 as the fuel and O_2 as the oxidant) with Si current collectors containing flow field channels with height and width less than 100 μm are examined with a Si microneedle surface functioning as the GDL (Publication V) and as a structure decreasing the contact resistance between a traditional carbon felt and the Si current collector (Publication VI). Furthermore, the use of MFCs as a catalyst sparing testing platform for new DMFC catalysts is shown to be viable (Publication IV).

6.1 Micro fuel cell fabrication

The small dimensions of the structures needed for MFCs require specialized fabrication procedures. The basis of this technology comes from the Si semiconductor industry, which later expanded to non-electronic devices termed micro electromechanical systems (MEMS). First miniaturized H_2-PEMFC and DMFC systems were presented in the early 2000s [241-243]. The aim in MFCs is to minimize the total volume of the system while preserving high power density by using small structures and thin components. The fabrication procedure involves designing the required structures on a mask, transferring this mask to a photoresist (optical lithography), etching of exposed areas of the substrate and possible surface coating. Due to the semiconductor industry roots, the substrate for the fabrication is commonly a Si wafer that should be doped to increase its conductivity so it can work as a current collector in MFC applications. Alternatively, undoped Si can be used if a conductive metal layer is deposited as a current collector. Other substrates can also be utilized including more conductive and robust metals (steel [244,245], aluminum [246]) and flexible metallized polymers (polymethyl methacrylate [247], commercial epoxy SU-8 [248]).

6.1.1 Optical litography

Photomask manufacture is a commercial process where the design of the microstructured object is replicated on a mask, which either blocks or allows light through where the microstructure will be etched. The substrate, commonly Si wafer, is covered with a photoresist, which after light exposure either becomes insoluble (negative resist) or soluble (positive resist) to certain mixtures called developer solutions. A common positive resist is a mixture of diazoquinone and Novolac resin, in which hydrophobic diazoquinone inhibits hydrophilic Novolac dissolution until it is exposed to light and becomes hydrophilic allowing the resist to be dissolved in alkaline solutions. Negative resists commonly polymerize in light rendering them insoluble (e.g. SU-8).

6.1.2 Etching

Etching of the patterned substrate is based on the slow etching of the photoresist, while the exposed substrate is quickly etched forming structures that can be less than a micrometer deep. One important feature of the etching is its directionality (Figure 19). Isotropic etch means that the substrate material is consumed at the same rate at all directions producing semi-circular structures. Anisotropic etch is a degree or two faster in certain directions or towards certain crystal planes of the substrate allowing the formation of deep structures with vertical walls. The different etch types were used Publication V to fabricate several kinds of flow channels for H_2-MFC.

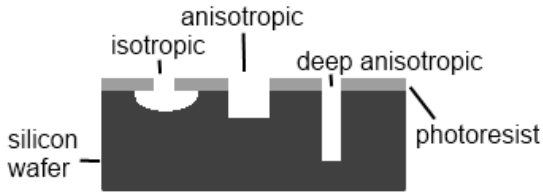

Figure 19. Schematics of the different etching types and structures they form on silicon substrate patterned with photoresist.

The etching method used in Publications IV-VI is called reactive ion etch (RIE), which is based on the basic principle that a gas is transformed into plasma by collisions with excited electrons. Most of the gas molecules will be in an excited state while some will even ionize. The gas must be chosen so that the plasma molecules form a volatile compound when they interact the substrate. In this case, the etching gas is SF_6 that combines with Si to form SiF_4 (boiling point -90°C). The etching can be anisotropic if the plasma contains enough ions or there are inhibitor molecules present in the

plasma. The ions move perpendicular in the electric field of the plasma chamber and impinge on the bottom of the structures being etched. Some ionic species can increase the etch rate of the etchant species (*e.g.* Ar^+ with XeF_2 on Si) causing the bottom of the structure to etch 10 to 100 times faster than the sides of the structure, where ions do not impinge. Inhibitors addition affects the process so that the ions remove the inhibitor layer from the bottom of the structure, while the sides of the structure remain protected. Si can be etched this way by the combination of SF_6 and O_2, since oxygen forms a passive oxyfluoride layer on the Si surface (Publications IV-VI), which requires low temperatures since oxyfluoride is only stable at less than -100°C. This method is called deep RIE (DRIE) because of the large depth achievable (Figure 19). Finally, isotropic etching can be achieved when the passivating species is absent or the temperature is too high for the passivating layer (Publication IV). The RIE etching processes used in this thesis were realized with an Oxford Instruments Plasmalab System 100 apparatus.

Silicon nanograss

Silicon nanograss is a term used to describe needle-like structures on Si surface (Figure 20), when the passivating conditions in RIE are enhanced. In practice, this means that the O_2 content of the plasma is raised to increase the oxyfluoride formation, while the ion energy of the plasma is decreased by lowering the bias voltage causing the ion bombardment. This means that the formation of the passivating layer is so high that the ions cannot remove it all resulting in Si needle structure shown in Figure 20. The shape of the needles can be changed by changing the operation parameters of the RIE (SF_6/O_2 ratio, temperature, pressure) [249]. Silicon nanograss is also called "black silicon" due to its ability to trap light between the needles making it appear completely black when compared to the high reflectivity of polished Si. This nanograss structure was used in Publications IV and V as the GDL of the MFC and in Publication VI to enhance the contact between the Si flow field and a carbon felt GDL.

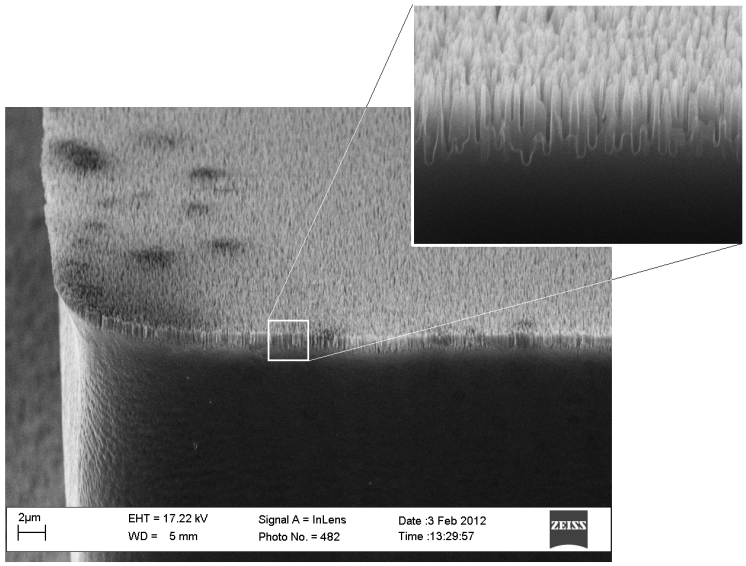

Figure 20. SEM image of silicon nanograss structure on top of a flow field pillar. (Publication VI)

6.1.3 Surface coating

The microstructures can be coated with various techniques (e.g. sputtering, atomic layer deposition, electroplating, spin coating) and substances to enhance their properties. In Publication V, the fabricated flow fields were sputtered with Pt and Cr to compare their performance. From these results there was no significant difference between the metals enabling the use of cheap Cr instead of more expensive metals for improved conductivity and corrosion resistance of the flow field. The use of highly boron-doped Si also enabled the use of thin Cr layers (30 nm compared to 200 nm Au), since it was not required for current collecting and thus, Cr was later used in other MFC tests (Publication IV) [250]. In Publication VI, more expensive Au was used instead, because of the sputtering device used for Cr was unavailable.

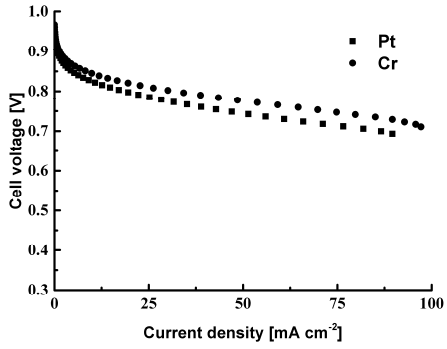

Figure 21. The polarization curves of room temperature silicon H_2-MFCs with Pt and Cr sputtered as the conductive protection layer on the flow field. Gas flows 50 ml min^{-1} of humidified H_2 and O_2.

6.2 Special constructions for micro fuel cells

6.2.1 Gas diffusion layer

Microfabrication techniques offer some options for integrating the GDL to the structure instead of using separate components like the carbon cloths of the larger cells. As the dimensions of the MFCs should be kept as small as possible, it is advantageous to replace the relatively thick carbon GDL (200-400 μm thick) with microstructures directly fabricated on the flow field or the membrane. Despite these limitations, carbon cloth, felt and paper have been previously used in MFC systems due to their effective mass transfer properties (Publication VI) [251-253].

A pseudo GDL can be formed by simply forming holes on the micrometer scale in the Si flow field structure. This allows the reactants to reach the CL and is especially useful for free-breathing MFCs taking O_2 directly from the atmosphere. For example pores of 10 μm in diameter and 200 μm in height penetrated into the current collector were determined to be suitable for a free-breathing ethanol fuel cell [254]. The design relies on the porosity of the CL and the small dimensions to effectively spread the reactant between the pores. The same applies for flow fields with channels and ridges (Figure 3), where the area under the ridges is not easily reached by the reactants.

Reactant flow under the ridges of the flow field can be enhanced by forming a porous structure on the top of them. In Publication V, silicon nanograss (Figure 20) was used as a carbon cloth replacement in H_2-MFCs with different flow field designs (Figure 22). The nanograss is only few micrometers tall and few hundred nanometers in diameter making the GDL very thin. The performances of these MFCs were superior to a similar design (∅2 μm, height 20 μm, 50 mA cm^{-2} at 0.3 V) reaching current of 50 mA cm^{-2} at 0.8 V (Figure 23) and clearly superior to larger Si pillars (∅30 μm, height 100 μm, 25 mA cm^{-2} at 0.3 V) [255], while their fabrication was relatively straight-forward compared to the other designs. This proved the feasibility of silicon nanograss as a GDL for MFCs, however, the high performance of the rectangular flow field could not be sustained. At about 100 mA cm^{-2} a sudden, irreversible decrease of current took place and the afterwards the current remained under 10 mA cm^{-2} at all temperatures. Drying and changing of the MEA did not recover this reproducible loss of performance nor was any obvious differences to new MFCs found with SEM, atomic force microscopy and Raman spectroscopy analysis. The crested profile performed slightly better than the pillar type but the very small contact area between the membrane and the silicon nanograss decreased the importance of a GDL, so therefore, later experiments were made with the rectangular pillar type flow fields (Publications IV and VI).

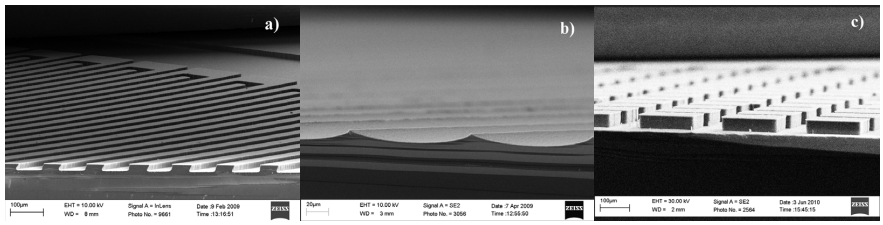

Figure 22. SEM images of the flow field profiles for MFCs used in Publication V. a) rectangular, b) crested, c) pillar

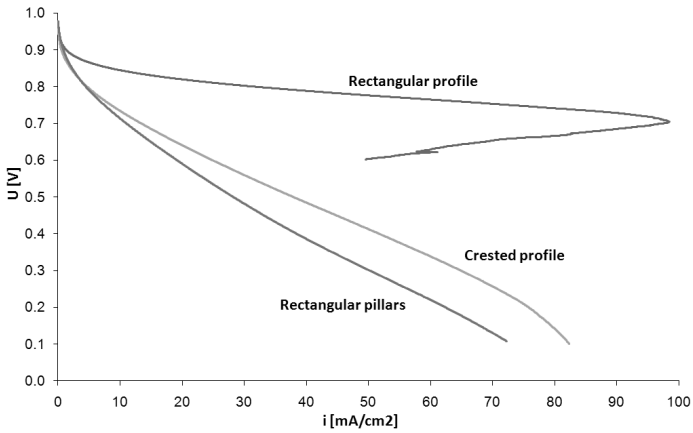

Figure 23. The polarization curves for 3 different flow field designs with silicon nanograss as the GDL. H_2-MFC operation with 50 ml min^{-1} flows of humidified gases at room temperature. (Publication V)

The porous layer can also be deposited on the ridges as an active layer. Yeom *et al.* [256] formed porous Pt black on Si mesh and used the structure as an integrated current collector and GDL for H_2-MFC and micro-DMFC. They found severe mass transfer limitation at 70 mA cm^{-2} for the H_2-MFC operation indicating that the small pores of the Pt layer are not efficient enough for water removal. For the DMFC operation no mass transfer limitation were found as only 10 times smaller current densities were achieved. Further tests with formic acid showed larger current than with the H_2-MFC and no mass transfer limitations, however they did not speculate on the reason of the enhanced mass-transfer with the liquid fuel. Kuriyama *et al.* [257] used a similar technique but first grew MWCNTs *in-situ* to their MFC current collector for GDL function and then deposited Pt on these MWCNT. Finally, metal foils can be etched to create highly conductive GDLs. Zhang *et al.* [258] etched thin Cu foil (12.5 μm) to a very porous structure and used it as GDL in a H_2-MFC. They measured very high performance (200 mA cm^{-2} at 0.8 V), but their membrane was thinner than the standard Nafion in Publication V (25 vs 120 μm). In addition their measurements were

performed at 70°C instead of room temperature explaining the excellent performance compared to the other experimental GDLs.

6.2.2 Silicon nanograss as performance enhancer with a carbon felt GDL

Since the silicon nanograss GDL is very thin (max 2 μm), it may not cope with the high water production at high current densities as the only GDL and thus its purpose was changed to a contact enhancer between fuel cell components in Publication VI due to its high surface area. Carbon felt (E-Tek ELAT® GDL LT1200N) with a microporous carbon layer on the membrane side was selected to be used as the GDL and the contact resistance between it and the flow fields with and without silicon nanograss were measured. The measurements were made with a construction where a bulky Cu cylinder (40 g) pressed the carbon felt against the flow field and the resistance was measured with a current sweep from 0 to 30 mA. Total resistance of the construct in the silicon nanograss case was 6.9±1.4 Ω, while in the smooth case it was 9.6±2.3 Ω indicating that silicon nanograss improves the electrical contact. The resistance also includes the bulk resistances of the Cu cylinder and the Si chip (small compared to the total values) and the constant value of the contact resistance between the copper cylinder and the microporous side of the GDL.

The effect of silicon nanograss on a H_2-MFC was then studied with a commercial Gore Primea MEA and a silicon chip design, where the flow field was etched into a recess to accommodate the relatively thick carbon felt GDL into the structure without causing fuel and oxidant leakage. The polarization curves measured for flow fields both with and without silicon nanograss are presented in Figure 24.

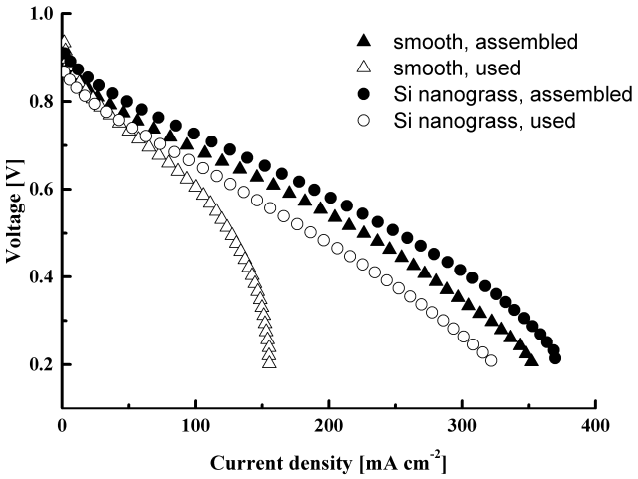

Figure 24. Polarization curves for H_2 -MFCs at room temperature with a carbon felt GDL. Triangles refer to MFCs with smooth flow field surface and circles to MFCs with silicon nanograss on the flow field. Filled symbols refer to just assembled MFCs and open symbols after 20 h chronoamperometric measurements at 0.4 V. (Publication VI)

The silicon nanograss equipped MFC showed improved performance but after measuring the cell for 20 h it became obvious that the enhancement was due to mass-transfer effects instead of lower contact resistance as the performance at high current densities decreased rapidly for the smooth MFCs. However, when cyclic voltammograms were measured, the water management seemed to be worse for the just assembled silicon nanograss MFC according to the large hysteresis between the forward and backward scans (Figure 25). After the 20 h measurement, the hysteresis was very small for both MFC types indicating that they had been saturated with water during the constant flow of humidified gases and the water generated in the cathode reaction. Moreover, since the achieved current densities also decreased, there was less water produced at the cathode resulting in a smaller effect of the mass transfer. The initial problems with silicon nanograss were attributed to the fact that according to SEM images part of it breaks down during fuel cell assembly and the broken shards may hinder the mass-transfer. Over time, these shards could be pushed out by the gas flow. The improved performance of the silicon nanograss MFC after usage could be due to its more hydrophilic nature: the contact angle on the flow field with silicon nanograss was 41° after a 15 min water immersion, while it was 77° for the smooth flow field. On a hydrophilic flow field surface the water forms a thin film and is pushed towards the cell outlets by the reactant flow [259]. Water is also more likely to leave from the GDL surface to the flow field wall and thus release GDL area for reactant transport. On the other hand, due to the pillar type flow field used in Publication VI, the droplets that form on more hydrophobic surfaces are not as easily pushed out of the cell due to the reactant pressure building behind them as in single serpentine channels of other flow field types (Figure 3). It is also possible that the more intimate contact

between the flow field and the GDL allows for better connection after the MFC is fully humidified.

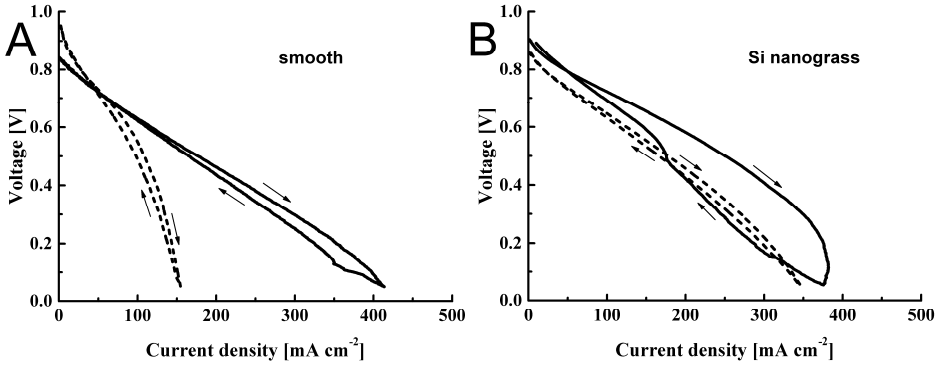

Figure 25. Cyclic voltammograms of H_2-MFCs at room temperature with a carbon felt GDL. A) with silicon nanograss on the flow field, B) smooth flow field surface. Solid line: just assembled MFCs (after polarization curves measurements in Figure 24), dashed line: after 20 h chronoamperometric measurement at 0.4 V. (Publication VI)

6.3 Micro fuel cells as a catalyst thrift tool

Often in testing new catalysts and membranes, the amount of the new material is limited due to unoptimized synthesis processes or the need to synthesize many materials for characterization. Testing of electrochemically active catalysts in a 3-electrode cell (Chapter 3.1) is one option for quick screening before moving to actual fuel cell tests. However, the active areas of the commercial fuel cell testing equipment are usually in the range of 5-25 cm^2, which means that large catalyst amounts are required especially for DMFC anode testing (1-4 mg cm^{-2}). In this respect, we tested MFCs as small active area test cells (Publication IV) and compared the results to a catalyst study made in our laboratory with a larger DMFC (macro-DMFC) for the same catalysts [33]. The active area of the MFCs was 1 cm^2, while it was 7.29 cm^2 for the macro-DMFC system. This is by no means the lower limit for MFC as our design has also been used with a 0.4 cm^2 active area and MFC structures are in the range of tens of micrometers enabling further decrease in the active area (flow field). The smallest MFCs fabricated are 0.1 cm^2 in size (corresponding to 3 x 3 mm square) [260]. MFCs also enable the quick and cheap fabrications of different flow field models that may be required in fuel cell testing.

The results in Publication IV and [33] indicate that the performances of the micro- and the macro-DMFC did not agree completely with each other and the performance order of the different catalyst supports were the opposite of each other (Table 1). In the macro DMFC, the order of current densities drawn from the cell was Vulcan > GNF > FWCNT,

while it was FWCNT > GNF > Vulcan for the micro-DMFC. The stability of the Vulcan and the FWCNT corresponded quite well between the tests, while the GNF was the most stable in the macro-DMFC and the least stable in the micro-DMFC. However, the micro-DMFC results correlated well with the chronoamperometric behavior of the catalyst in the 3-electrode cell [33] showing similar current decreases.

However, a few experimental details were different between the DMFC measurements due to unavoidable circumstances. Firstly, the measurements temperature was 70°C for the macro-DMFC, while it was 30°C for the micro-DMFC due to an inadequate heating arrangement. The GDL was also different as the carbon cloth used in the larger DMFC was replaced with the silicon nanograss GDL in the MFC. Finally, the OCV of the Vulcan-supported catalyst was so low (0.37 V) that the chronoamperometric measurements were made at lower potential than in the larger DMFC (0.2 vs 0.4 V) probably due to the unoptimal isolation of the MFC cathode and anode. These differences underscore that the MFC structure and measurements have to be carefully considered to be able to match the larger fuel cells in order to have comparable results. For example, the relatively large secondary pores of the GNF- and FWCNT-supported CL may be advantageous for the mass-transfer methanol and CO_2 and this is emphasized with the silicon nanograss GDL that is not as effective as a carbon cloth or felt GDL thus downplaying the performance of the Vulcan-supported CL.

Table 1. The maximum current densities of the micro (@ 0.1 V) and macro (@ 0.05 V) DMFC with different PtRu supports on the anode before and after 137 h (macro) and 72 h (micro) chronoamperometric test at 70°C (macro) and 30°C (micro). The numbers in parenthesis show the performance order of the catalyst supports. Macro-DMFC results from [33] and micro-DMFC results from Publication IV.

Catalyst support	**Initial macro-DMFC activity**	**Final macro-DMFC activity**	**Macro-DMFC stability**	**Initial micro-DMFC activity**	**Final micro-DMFC activity**	**Micro DMFC stability**
	mA cm^{-2}	mA cm^{-2}		mA cm^{-2}	mA cm^{-2}	
Vulcan	299 (1)	257 (1)	14%	35 (3)	31 (3)	11%
GNF	231 (2)	229 (2)	1%	111 (2)	69 (2)	38%
FWCNT	158 (3)	103 (3)	35%	151 (1)	113 (1)	25%

7. Conclusions

This thesis investigates the issues regarding the application of DMFCs and H_2-PEMFCs for portable power systems from the perspective of structures in both the catalytic materials and the miniaturized flow field and current collector. New, more powerful catalysts for MOR and ORR reactions in the DMFC were studied emphasizing their application in the actual fuel cell environment to understand all the differences they have compared to current commercial catalysts. Novel microstructures were tested in micro fuel cells with standard materials to cheapen and simplify their fabrication with higher performance. Finally, new catalysts were directly tested in a micro-DMFC and the results were compared to similar tests performed in a laboratory-scale test DMFC.

FWCNTs were examined in several roles in this thesis due to their interesting properties that combine the structural perfection of SWCNTs and the robustness of MWCNTs. It was found that they are efficient in immobilizing redox active biomolecule PQQ most likely as a result of the favorable π–π interactions between the benzene rings in both. The FWCNTs also formed an entangled and porous structure on the electrode, which may help to capture more PQQ. Immobilized PQQ can be used to prepare high concentration enzyme electrodes and to facilitate to electron transfer between the enzyme and electrode. The FWCNT were also found to be a good support material for PtRu nanoparticles as the catalyst particle distribution was narrower and the average particle size smaller than on a standard carbon black support. This MOR catalyst performed 6 times better in the micro-DMFC test than the carbon black supported catalyst and showed minimal changes in the particle size and CL structure after a 72 h test. Finally, the N-doping of FWCNTs produced a very active and methanol tolerant ORR catalyst, which was tested in an alkaline DMFC and resulted in 4 times better performance than Pt. All in all, FWCNTs appear to be a highly promising starting material for electrochemical catalyst.

The effect of new catalyst materials on the CL structure and optimization was also studied for a number of cases. When the support material of PtRu was changed from carbon black to GNF to FWCNT, clear differences in the Nafion-based CL structure

could be seen from the SEM images. Carbon black forms a sponge like structure with small secondary pores, while GNF shows large secondary pores penetrating deeply into the CL. For FWCNT, the CL seems to be formed from agglomerates of catalyst and Nafion and cracks between these agglomerates allow reactant flow through the layer. The agglomeration was more pronounced when FWCNT were doped with nitrogen and used as an ORR catalyst in the alkaline DMFC and the secondary pores between the agglomerates were larger. It seems that the inherent charge caused by the nitrogen atoms attracts the ionomer even more strongly around the catalyst during CL formation. It is clear that such a radically different structure affects the mass transport properties of the CL. This was further studied by optimizing the Nafion content of a GNF-PtRu based anode. It was found out that the optimum amount of Nafion was 50 wt% and the DMFC functioned properly even with 70 wt%, which is much higher than the optimum for commercial carbon black supported catalysts (20-40 wt%). Similar result was obtained with N-doped FWCNTs as their optimum ionomer content was 40 wt% in the alkaline DMFC. The finding clearly demonstrate that the large secondary pores enhance the mass transport and therefore it is possible to use a higher amount of ionomer resulting in better long-term stability during a 220 h test with Nafion and GNF-PtRu.

As they are very important for miniaturization of the whole power system, MFCs were investigated for the replacement and use of standard fuel cell components in a H_2-fueled system. A special Si nanograss structure was shown to be a possible alternative for a GDL in micro fuel cells thus simplifying the assembly of the cell as it is an integrated structure unlike carbon felts or papers commonly used. It was also discovered that for the protection and conductivity enhancement, an expensive Pt thin film coating was not necessary but Cr could perform just as well. However, the fuel cell suffered from irreversibly degradation with this GDL at high current densities, so its purpose was changed to be a high area contact surface to a carbon felt GDL. Measurements indicated that Si nanograss decreased the contact resistance between the current collector and the GDL. Moreover, it was shown that it aided in the water management of the cell during a 1-day test demonstrating that innovative combinations of traditional and novel components and structures can result in improved performance of the whole system. However, the Si nanograss GDL was still used with the micro-DMFCs because the current densities were lower. Additionally, it was studied whether the micro-DMFCs could replicate the results obtained on a larger test DMFC in order to save catalyst due to the lower active area of the micro fuel cells. Some measurement parameters had to be changed because the systems were so different and deviating results were obtained. It was concluded that in order to use one system to predict the DMFC behavior in another system, the measurements should be carefully controlled to mimic each other as much as possible as even small changes in the

components or conditions can lead to widely different performance, which is furthermore dependent on the MEA structure and its interaction with the other components.

7.1 Recommendations for further work

Carbon supports are not limited to what is researched in this thesis, for example mesoporous carbon and graphene are studied widely and have interesting features for fuel cell testing. The properties of the supports can be changed by doping with heteroatoms and, as was seen for the case of N-doped FWCNT, this can have large effects on the CL structure. These catalysts could then be used as either the supports for different metals in MOR or as they are in ORR. A dedicated fuel cell system with the possibility to do stability measurements over thousands of hours on many samples at the same time with variable loading patterns would also give more insight into the degradation mechanism of the MEA. The measurements could be improved by incorporating a real reference electrode within the fuel cell system to make it a 3-electrode cell as the cathode functioning as a dynamic hydrogen electrode still polarizes due to the current going through it. This would enable more accurate measurements of the electrode of interest. Also, a more detailed look at the CL pore structure could be made with for example mercury intrusion porosimetry and the effect of catalyst supports further elucidated.

For the micro fuel cells, materials other than Si would be interesting to study. Some preliminary measurements with Al-based hydrogen fuel cells have been made with very high performance (maximum power density 250 mW cm^{-2} [246]) and it would be interesting to continue to test them with different flow field designs to see if the performance could be further improved without the degradation and fragility seen with Si. In addition, vertical stacking of these cells to produce higher voltage and power has proven to be challenging and new strategies should be devised to improve their durability and to reduce leaking.

References

[1] K.A. Mauritz, R.B. Moore, *Chem. Rev.* **104** (2004) 4535-4586.

[2] H. Yang, T.S. Zhao, *Electrochim. Acta* **50** (2005) 3243-3252.

[3] S. Park, J. Lee, B.N. Popov, *Int. J. Hydrogen Energy* **37** (2012) 5850-5865.

[4] E.H. Yu, U. Krewer, K. Scott, *Energies (Basel, Switz.)* **3** (2010) 1499-1528.

[5] K. Scott, E. Yu, G. Vlachogiannopoulos, M. Shivare, N. Duteanu, *J. Power Sources* **175** (2008) 452-457.

[6] F. Lufrano, V. Baglio, P. Staiti, V. Antonucci, A.S. Aricó, *J. Power Sources* **243** (2013) 519-534.

[7] E. Agel, J. Bouet, J.F. Fauvarque, *J. Power Sources* **101** (2001) 267-274.

[8] W.T. Grubb, US Patent, 2,913,511 (1959).

[9] G. Fabricius, S. Liukkonen, G. Sundholm, Fysikaalisen kemian taulukoita, Otatieto, Helsinki; 1994, pp. 104.

[10] C. Coutanceau, L. Demarconnay, C. Lamy, J.-M. Léger, *J. Power Sources* **156** (2006) 14-19.

[11] M.S. Naughton, F.R. Brushett, P.J.A. Kenis, *J. Power Sources* **196** (2011) 1762-1768.

[12] Y. Wang, L. Li, L. Hu, L. Zhuang, J. Lu, B. Xu, *Electrochem. Commun.* **5** (2003) 662-666.

[13] J.L. Cohen, D.J. Volpe, H.D. Abruna, *Phys. Chem. Chem. Phys.* **9** (2007) 49-77.

[14] K.N. Grew, X. Ren, D. Chu, *ECS Trans.* **41** (2011) 1979-1985.

[15] S.J. Ewing, R. Lan, X.X. Xu, S.W. Tao, *Fuel Cells* **10** (2010) 72-76.

[16] J.R. Varcoe, R.C.T. Slade, G.L. Wright, Y. Chen, *J. Phys. Chem. B* **110** (2006) 21041-21049.

[17] K. Miyazaki, N. Sugimura, K. Matsuoka, Y. Iriyama, T. Abe, M. Matsuoka, Z. Ogumi, *J. Power Sources* **178** (2008) 683-686.

[18] M. Ahmed, I. Dincer, *Int. J. Energy Res.* **35** (2011) 1213-1228.

[19] T. Tschinder, T. Schaffer, S.D. Fraser, V. Hacker, *J. Appl. Electrochem.* **37** (2007) 711-716.

[20] S.H. Seo, C.S. Lee, *Energy Fuels* **22** (2008) 1212-1219.

[21] S. Yousefi, M. Zohoor, *Ionics* **19** (2013) 1195-1201.

[22] G. Jung, A. Su, F. Weng, C. Tu, *J. Fuel Cell Sci. Tech.* **2** (2004) 81-85.

[23] V. Saarinen, T. Kallio, M. Paronen, P. Tikkanen, E. Rauhala, K. Kontturi, *Electrochim. Acta* **50** (2005) 3453-3460.

[24] S. Slade, S.A. Campbell, T.R. Ralph, F.C. Walsh, *J. Electrochem. Soc.* **149** (2002) A1556-A1564.

[25] H. Dohle, J. Divisek, R. Jung, *J. Power Sources* **86** (2000) 469-477.

[26] J. Ge, H. Liu, *J. Power Sources* **142** (2005) 56-69.

[27] Z. Guo, A. Faghri, *J. Power Sources* **160** (2006) 1142-1155.

[28] S.L. Gojković, S. Gupta, R.F. Savinell, *J. Electroanal. Chem.* **462** (1999) 63-72.

[29] R.W. Reeve, P.A. Christensen, A. Hamnett, S.A. Haydock, S.C. Roy, *J. Electrochem. Soc.* **145** (1998) 3463-3471.

[30] N.M. Marković, H.A. Gasteiger, P.N. Ross Jr, X. Jiang, I. Villegas, M.J. Weaver, *Electrochim. Acta* **40** (1995) 91-98.

[31] W.L. Holstein, H.D. Rosenfeld, *J. Phys. Chem. B* **109** (2005) 2176-2186.

[32] J. Leger, B. Beden, C. Lamy, S. Bilmes, *J. Electroanal. Chem. Interfacial Electrochem.* **170** (1984) 305-317.

[33] A. Santasalo-Aarnio, M. Borghei, I.V. Anoshkin, A.G. Nasibulin, E.I. Kauppinen, V. Ruiz, T. Kallio, *Int. J. Hydrogen Energy* **37** (2012) 3415-3424.

[34] M. Borghei, P. Kanninen, M. Lundahl, I. Anoshkin, T. Susi, J. Sainio, A. Nasibulin, T. Kallio, K. Tammeveski, E. Kauppinen, V. Ruiz, *Appl. Catal. , B* (2014) doi:10.1016/j.apcatb.2014.04.027.

[35] Z. Wang, X. Wang, P. Zuo, B. Yang, G. Yin, X. Feng, *J. Power Sources* **181** (2008) 93-100.

[36] M.S. Wilson, S. Gottesfeld, *J. Electrochem. Soc.* **139** (1992) L28-L30.

[37] M. Carmo, G. Doubek, R.C. Sekol, M. Linardi, A.D. Taylor, *J. Power Sources* **230** (2013) 169-175.

[38] J.B. Lakeman, G.O. Mepsted, P.L. Adcock, P.J. Mitchell, J.M. Moore, *J. Power Sources* **65** (1997) 179-185.

[39] A. Hamnett, The components of an electrochemical cell. In: Vielstich W, Lamm A, Gasteiger HA, (Eds), Handbook of Fuel Cells: Fundamentals, Technology and Applications, Wiley, 2003, pp. 3-12.

[40] T. Iwasita, *Electrochim. Acta* **47** (2002) 3663-3674.

[41] A. Santasalo, F.J. Vidal-Iglesias, J. Solla-Gullón, A. Berná, T. Kallio, J.M. Feliu, *Electrochim. Acta* **54** (2009) 6576-6583.

[42] P.S. Kauranen, E. Skou, J. Munk, *J. Electroanal. Chem.* **404** (1996) 1-13.

[43] H. Hanawa, K. Kunimatsu, H. Uchida, M. Watanabe, *Electrochim. Acta* **54** (2009) 6276-6285.

[44] G. Garcia, M.T.M. Koper, *Phys. Chem. Chem. Phys.* **10** (2008) 3802-3811.

[45] E. Herrero, Q. Chen, J. Hernandez, S. Sun, J.M. Feliu, *Phys. Chem. Chem. Phys.* **13** (2011) 16762-16771.

[46] T. Kobayashi, P.K. Babu, L. Gancs, J.H. Chung, E. Oldfield, A. Wieckowski, *J. Am. Chem. Soc.* **127** (2005) 14164-14165.

[47] P.K. Babu, J.-H. Chung, E. Oldfield, A. Wieckowski, *Electrochim. Acta* **53** (2008) 6672-6679.

[48] M. Götz, H. Wendt, *Electrochim. Acta* **43** (1998) 3637-3644.

[49] W.J. Zhou, B. Zhou, W.Z. Li, Z.H. Zhou, S.Q. Song, G.Q. Sun, Q. Xin, S. Douvartzides, M. Goula, P. Tsiakaras, *J. Power Sources* **126** (2004) 16-22.

[50] I. Ávila-García, C. Ramírez, J.M. Hallen López, E.M. Arce Estrada, *J. Alloys Compd.* **495** (2010) 462-465.

[51] A. Crown, I.R. Moraes, A. Wieckowski, *J. Electroanal. Chem.* **500** (2001) 333-343.

[52] T. Page, R. Johnson, J. Hormes, S. Noding, B. Rambabu, *J. Electroanal. Chem.* **485** (2000) 34-41.

[53] X. Zhang, K. Tsang, K. Chan, *J. Electroanal. Chem.* **573** (2004) 1-9.

[54] K. Park, J. Choi, B. Kwon, S. Lee, Y. Sung, H. Ha, S. Hong, H. Kim, A. Wieckowski, *J. Phys. Chem. B* **106** (2002) 1869-1877.

[55] B. Gurau, R. Viswanathan, R. Liu, T.J. Lafrenz, K.L. Ley, E.S. Smotkin, E. Reddington, A. Sapienza, B.C. Chan, T.E. Mallouk, S. Sarangapani, *J. Phys. Chem. B* **102** (1998) 9997-10003.

[56] E. Reddington, A. Sapienza, B. Gurau, R. Viswanathan, S. Sarangapani, E.S. Smotkin, T.E. Mallouk, *Science* **280** (1998) 1735-1737.

[57] O. Petrii, *J. Solid State Electrochem.* **12** (2008) 609-642.

[58] L. Gao, H. Huang, C. Korzeniewski, *Electrochim. Acta* **49** (2004) 1281-1287.

[59] S. Wasmus, J.-T. Wang, R.F. Savinell, *J. Electrochem. Soc.* **142** (1995) 3825-3833.

[60] I. Tkach, A. Panchenko, T. Kaz, V. Gogel, K.A. Friedrich, E. Roduner, *Phys. Chem. Chem. Phys.* **6** (2004) 5419-5426.

[61] L. Gancs, N. Hakim, B. Hult, S. Mukerjee, *ECS Trans.* **3** (2006) 607-618.

[62] X. Wang, W. Li, Z. Chen, M. Waje, Y. Yan, *J. Power Sources* **158** (2006) 154-159.

[63] P. Joghee, S. Pylypenko, T. Olson, A. Dameron, A. Corpuz, H.N. Dinh, K. Wood, K. O'Neill, K. Hurst, G. Bender, T. Gennett, B. Pivovar, R. O'Hayre, *J. Electrochem. Soc.* **159** (2012) F768-F778.

[64] S. Pylypenko, A. Borisevich, K.L. More, A.R. Corpuz, T. Holme, A.A. Dameron, T.S. Olson, H.N. Dinh, T. Gennett, R. O'Hayre, *Energy Environ. Sci.* **6** (2013) 2957-2964.

[65] C. Anthony, *Biochem. J.* **320** (1996) 697-711.

[66] E.V. Plotkin, I.J. Higgins, H.A.O. Hill, *Biotechnol. Lett.* **3** (1981) 187-192.

[67] G.T.R. Palmore, H. Bertschy, S.H. Bergens, G.M. Whitesides, *J. Electroanal. Chem.* **443** (1998) 155-161.

[68] X. Zhang, A. Ranta, A. Halme, *Biosens. Bioelectron.* **21** (2006) 2052-2057.

[69] C.M. Moore, S.D. Minteer, R.S. Martin, *Lab Chip* **5** (2005) 218-225.

[70] Y. Yan, I. Baravik, R. Tel-Vered, I. Willner, *Adv. Mater.* **21** (2009) 4275-4279.

[71] S. Aquino Neto, J.C. Forti, V. Zucolotto, P. Ciancaglini, A.R. de Andrade, *Biosens. Bioelectron.* **26** (2011) 2922-2926.

[72] P.G. Fenga, F.P. Cardoso, S. Aquino Neto, A.R. De Andrade, *Electrochim. Acta* **106** (2013) 109-113.

[73] N.L. Akers, C.M. Moore, S.D. Minteer, *Electrochim. Acta* **50** (2005) 2521-2525.

[74] A. Ramanavicius, A. Kausaite, A. Ramanaviciene, *Biosens. Bioelectron.* **24** (2008) 761-766.

[75] S. Aquino Neto, E.L. Suda, S. Xu, M.T. Meredith, A.R. De Andrade, S.D. Minteer, *Electrochim. Acta* **87** (2013) 323-329.

[76] S. Zhao, R.B. Lennox, *Anal. Chem.* **63** (1991) 1174-1178.

[77] E.C.A. Stigter, G.A.H. de Jong, J.A. Jongejan, J.A. Duine, J.P. van der Lugt, W.A.C. Somers, *Enzyme Microb. Technol.* **18** (1996) 489-494.

[78] A. Ramanavicius, K. Habermüller, E. Csöregi, V. Laurinavicius, W. Schuhmann, *Anal. Chem.* **71** (1999) 3581-3586.

[79] W. Schuhmann, H. Zimmermann, K. Habermuller, V. Laurinavicius, *Faraday Discuss.* **116** (2000) 245-255.

[80] M. Zayats, E. Katz, R. Baron, I. Willner, *J. Am. Chem. Soc.* **127** (2005) 12400-12406.

[81] D. Sun, D. Scott, M.J. Cooney, B.Y. Liaw, *Electrochem. Solid-State Lett.* **11** (2008) B101-B104.

[82] H. Shinohara, G.F. Khan, Y. Ikariyama, M. Aizawa, *J. Electroanal. Chem. Interfacial Electrochem.* **304** (1991) 75-84.

[83] A. Curulli, I. Carelli, O. Trischitta, G. Palleschi, *Biosens. Bioelectron.* **12** (1997) 1043-1055.

[84] E. Katz, D.D. Schlereth, H. Schmidt, *J. Electroanal. Chem.* **367** (1994) 59-70.

[85] M. Yamashita, C.A. Pessôa, L.T. Kubota, *J. Colloid Interface Sci.* **263** (2003) 99-105.

[86] H. Jao, P. Tsai, C.M. Wang, *J. Electroanal. Chem.* **606** (2007) 141-149.

[87] E.G. Rakov, D.A. Grishin, Y.V. Gavrilov, E.V. Rakova, A.G. Nasibulin, H. Jiang, E.I. Kauppinen, *Russ. J. Electrochem.* **78** (2004) 1966-1971.

[88] C. Qian, H. Qi, B. Gao, Y. Cheng, Q. Qiu, L. Qin, O. Zhou, J. Liu, *J. Nanosci. Nanotechnol.* **6** (2006) 1346-1349.

[89] K. Yang, B. Xing, *Chem. Rev.* **110** (2010) 5989-6008.

[90] J. Liu, O. Bibari, P. Mailley, J. Dijon, E. Rouviere, F. Sauter-Starace, P. Caillat, F. Vinet, G. Marchand, *New J. Chem.* **33** (2009) 1017-1024.

[91] P. Abiman, A. Crossley, G.G. Wildgoose, J.H. Jones, R. Compton G., *Langmuir* **23** (2007) 7847-7852.

[92] L. Minati, G. Speranza, I. Bernagozzi, S. Torrengo, L. Toniutti, B. Rossi, M. Ferrari, A. Chiasera, *J. Phys. Chem. C* **114** (2010) 11068-11073.

[93] S. Sharma, B.G. Pollet, *J. Power Sources* **208** (2012) 96-119.

[94] E. Antolini, *Appl. Catal. , B* **88** (2009) 1-24.

[95] M. Uchida, Y. Aoyama, M. Tanabe, N. Yanagihara, N. Eda, A. Ohta, *J. Electrochem. Soc.* **142** (1995) 2572-2576.

[96] K.H. Kangasniemi, D.A. Condit, T.D. Jarvi, *J. Electrochem. Soc.* **151** (2004) E125-E132.

[97] C.A. Reiser, L. Bregoli, T.W. Patterson, J.S. Yi, J.D. Yang, M.L. Perry, T.D. Jarvi, *Electrochem. Solid-State Lett.* **8** (2005) A273-A276.

[98] Z. Wang, T. Kotake, Y. Takagi, *ECS Trans.* **11** (2007) 1013-1019.

[99] A.A. Kulikovsky, *Electrochim. Acta* **56** (2011) 9846-9850.

[100] L.M. Roen, C.H. Paik, T.D. Jarvi, *Electrochem. Solid-State Lett.* **7** (2004) A19-A22.

[101] G. Álvarez, F. Alcaide, O. Miguel, P.L. Cabot, M.V. Martínez-Huerta, J.L.G. Fierro, *Electrochim. Acta* **56** (2011) 9370-9377.

[102] P. Serp, M. Corrias, P. Kalck, *Appl. Catal. , A* **253** (2003) 337-358.

[103] M. Carmo, V.A. Paganin, J.M. Rosolen, E.R. Gonzalez, *J. Power Sources* **142** (2005) 169-176.

[104] K. Jeng, C. Chien, N. Hsu, W. Huang, S. Chiou, S. Lin, *J. Power Sources* **164** (2007) 33-41.

[105] Z. Liu, X.Y. Ling, B. Guo, L. Hong, J.Y. Lee, *J. Power Sources* **167** (2007) 272-280.

[106] J. Prabhuram, T.S. Zhao, Z.X. Liang, R. Chen, *Electrochim. Acta* **52** (2007) 2649-2656.

[107] C.-H. Wang, H.-Y. Du, Y.-T. Tsai, C.-P. Chen, C.-J. Huang, L.C. Chen, K.H. Chen, H.-C. Shih, *J. Power Sources* **171** (2007) 55-62.

[108] M. Tsai, T. Yeh, C. Chen, C. Tsai, *Electrochem. Commun.* **9** (2007) 2299-2303.

[109] Z. Cui, C. Liu, J. Liao, W. Xing, *Electrochim. Acta* **53** (2008) 7807-7811.

[110] N. Hsu, C. Chien, K. Jeng, *Appl. Catal. , B* **84** (2008) 196-203.

[111] J. Drillet, H. Bueb, R. Dittmeyer, U. Dettlaff-Weglikowska, S. Roth, *J. Electrochem. Soc.* **156** (2009) F137-F144.

[112] P. Hernández-Fernández, R. Nuño, E. Fatás, J.L.G. Fierro, P. Ocón, *Int. J. Hydrogen Energy* **36** (2011) 8267-8278.

[113] J. Guo, G. Sun, Q. Wang, G. Wang, Z. Zhou, S. Tang, L. Jiang, B. Zhou, Q. Xin, *Carbon* **44** (2006) 152-157.

[114] M. Tsuji, M. Kubokawa, R. Yano, N. Miyamae, T. Tsuji, M.S. Jun, S. Hong, S. Lim, S.H. Yoon, I. Mochida, *Langmuir* **23** (2007) 387-390.

[115] E.S. Steigerwalt, G.A. Deluga, C.M. Lukehart, *J. Phys. Chem. B* **106** (2002) 760-766.

[116] G. Girishkumar, T.D. Hall, K. Vinodgopal, P.V. Kamat, *J. Phys. Chem. B* **110** (2006) 107-114.

[117] W. Tokarz, G. Lota, E. Frackowiak, A. Czerwiński, P. Piela, *Electrochim. Acta* **98** (2013) 94-103.

[118] S. Kang, S. Lim, D. Peck, S. Kim, D. Jung, S. Hong, H. Jung, Y. Shul, *Int. J. Hydrogen Energy* **37** (2012) 4685-4693.

[119] T. Frelink, W. Visscher, J.A.R. van Veen, *J. Electroanal. Chem.* **382** (1995) 65-72.

[120] T. Kim, S. Lim, K. Kwon, S. Hong, W. Qiao, C.K. Rhee, S. Yoon, I. Mochida, *Langmuir* **22** (2006) 9086-8.

[121] J.K. Nørskov, J. Rossmeisl, A. Logadottir, L. Lindqvist, J.R. Kitchin, T. Bligaard, H. Jónsson, *J. Phys. Chem. B* **108** (2004) 17886-17892.

[122] A. Damjanovic, M.A. Genshaw, J.O. Bockris, *J. Electrochem. Soc.* **114** (1967) 1107-1112.

[123] N.A. Anastasijević, V. Vesović, R.R. Adžić, *J. Electroanal. Chem. Interfacial Electrochem.* **229** (1987) 305-316.

[124] O. Antoine, R. Durand, *J. Appl. Electrochem.* **30** (2000) 839-844.

[125] H. Yano, J. Inukai, H. Uchida, M. Watanabe, P.K. Babu, T. Kobayashi, J.H. Chung, E. Oldfield, A. Wieckowski, *Phys. Chem. Chem. Phys.* **8** (2006) 4932-4939.

[126] L. Jiang, A. Hsu, D. Chu, R. Chen, *J. Electroanal. Chem.* **629** (2009) 87-93.

[127] L. Geniès, R. Faure, R. Durand, *Electrochim. Acta* **44** (1998) 1317-1327.

[128] A. Panchenko, H. Dilger, J. Kerres, M. Hein, A. Ullrich, T. Kaz, E. Roduner, *Phys. Chem. Chem. Phys.* **6** (2004) 2891-2894.

[129] S. Mu, C. Xu, Q. Yuan, Y. Gao, F. Xu, P. Zhao, *J. Appl. Polym. Sci.* **129** (2013) 1586-1592.

[130] C. Lamy, C. Coutanceau, N. Alonso-Vante, Methanol-Tolerant Cathode Catalysts for DMFC. In: Liu H, Zhang J, (Eds), Electrocatalysis of Direct Methanol Fuel Cells: From Fundamentals to Applications, 2009, pp. 257-314.

[131] I.E.L. Stephens, A.S. Bondarenko, U. Gronbjerg, J. Rossmeisl, I. Chorkendorff, *Energy Environ. Sci.* **5** (2012) 6744-6762.

[132] F. Jaouen, E. Proietti, M. Lefevre, R. Chenitz, J. Dodelet, G. Wu, H.T. Chung, C.M. Johnston, P. Zelenay, *Energy Environ. Sci.* **4** (2011) 114-130.

[133] R. Jasinski, *Nature* **201** (1964) 1212-1213.

[134] H. Wang, Côté R., G. Faubert, D. Guay, J.P. Dodelet, *J. Phys. Chem. B* **103** (1999) 2042-2049.

[135] M. Lefèvre, E. Proietti, F. Jaouen, J. Dodelet, *Science* **324** (2009) 71-74.

[136] E. Proietti, F. Jaouen, M. Lefèvre, N. Larouche, J. Tian, J. Herranz, J. Dodelet, *Nat. Commun.* **2** (2011) 416.

[137] K. Gong, F. Du, Z. Xia, M. Durstock, L. Dai, *Science* **323** (2009) 760-764.

[138] S. Maldonado, K.J. Stevenson, *J. Phys. Chem. B* **109** (2005) 4707-4716.

[139] P.H. Matter, L. Zhang, U.S. Ozkan, *J. Cat.* **239** (2006) 83-96.

[140] X. Li, G. Liu, B.N. Popov, *J. Power Sources* **195** (2010) 6373-6378.

[141] W. Yang, T. Fellinger, M. Antonietti, *J. Am. Chem. Soc.* **133** (2011) 206-209.

[142] Z. Mo, S. Liao, Y. Zheng, Z. Fu, *Carbon* **50** (2012) 2620-2627.

[143] J. Bai, Q. Zhu, Z. Lv, H. Dong, J. Yu, L. Dong, *Int. J. Hydrogen Energy* **38** (2013) 1413-1418.

[144] L. Qu, Y. Liu, J. Baek, L. Dai, *ACS Nano* **4** (2010) 1321-1326.

[145] D. Geng, Y. Chen, Y. Chen, Y. Li, R. Li, X. Sun, S. Ye, S. Knights, *Energy Environ. Sci.* **4** (2011) 760-764.

[146] S.M. Unni, S. Devulapally, N. Karjule, S. Kurungot, *J. Mater. Chem.* **22** (2012) 23506-23513.

[147] Z. Chen, D. Higgins, H. Tao, R.S. Hsu, Z. Chen, *J. Phys. Chem. C* **113** (2009) 21008-21013.

[148] T.C. Nagaiah, S. Kundu, M. Bron, M. Muhler, W. Schuhmann, *Electrochem. Commun.* **12** (2010) 338-341.

[149] Z. Wang, R. Jia, J. Zheng, J. Zhao, L. Li, J. Song, Z. Zhu, *ACS Nano* **5** (2011) 1677-1684.

[150] Y. Qiu, J. Yu, T. Shi, X. Zhou, X. Bai, J.Y. Huang, *J. Power Sources* **196** (2011) 9862-9867.

[151] R. Liu, D. Wu, X. Feng, K. Muellen, *Angew. Chem. , Int. Ed.* **49** (2010) 2565-2569, S2565/1-S2565/6.

[152] X. Zhou, Z. Yang, H. Nie, Z. Yao, L. Zhang, S. Huang, *J. Power Sources* **196** (2011) 9970-9974.

[153] Y.M. Yu, J.H. Zhang, C.H. Xiao, J.D. Zhong, X.H. Zhang, J.H. Chen, *Fuel Cells (Weinheim, Ger.)* **12** (2012) 506-510.

[154] M.S. Thorum, J.M. Hankett, A.A. Gewirth, *J. Phys. Chem. Lett.* **2** (2011) 295-298.

[155] D. von Dieter, D. Singh, J.C. King, U.S. Ozkan, *Appl. Catal. , B* **113-114** (2012) 126-133.

[156] V. Nallathambi, J. Lee, S.P. Kumaraguru, G. Wu, B.N. Popov, *J. Power Sources* **183** (2008) 34-42.

[157] G. Liu, X. Li, P. Ganesan, B.N. Popov, *Electrochim. Acta* **55** (2010) 2853-2858.

[158] T. Onodera, S. Suzuki, T. Mizukami, H. Kanzaki, *J. Power Sources* **196** (2011) 7994-7999.

[159] H. Oh, J. Oh, W.H. Lee, H. Kim, H. Kim, *Int. J. Hydrogen Energy* **36** (2011) 8181-8186.

[160] A. Dorjgotov, J. Ok, Y. Jeon, S. Yoon, Y. Shul, *J. Solid State Electrochem.* **17** (2013) 2567-2577.

[161] J. Kim, S. Lim, S. Kim, D. Peck, B. Lee, S. Yoon, D. Jung, *J. Nanosci. Nanotechnol.* **11** (2011) 6350-6358.

[162] D.C. Higgins, Z. Chen, *ECS Trans.* **28** (2010) 63-68.

[163] R. Venkateswara Chitturi, Y. Ishikawa, *J. Phys. Chem. C* **116** (2012) 4340-4346.

[164] X. Sun, P. Song, Y. Zhang, C. Liu, W. Xu, W. Xing, *Sci. Rep.* **3** (2013).

[165] Z. Yang, H. Nie, X. Chen, X. Chen, S. Huang, *J. Power Sources* **236** (2013) 238-249.

[166] A. Santasalo-Aarnio, S. Tuomi, K. Jalkanen, K. Kontturi, T. Kallio, *Electrochim. Acta* **87** (2013) 730-738.

[167] A.K. Shukla, C.L. Jackson, K. Scott, R.K. Raman, *Electrochim. Acta* **47** (2002) 3401-3407.

[168] R.K. Raman, G. Murgia, A.K. Shukla, *J. Appl. Electrochem.* **34** (2004) 1029-1038.

[169] A. Santasalo-Aarnio, S. Hietala, T. Rauhala, T. Kallio, *J. Power Sources* **196** (2011) 6153-6159.

[170] S. Litster, G. McLean, *J. Power Sources* **130** (2004) 61-76.

[171] E.A. Ticianelli, C.R. Derouin, A. Redondo, S. Srinivasan, *J. Electrochem. Soc.* **135** (1988) 2209-2214.

[172] M.S. Wilson, S. Gottesfeld, *J. Appl. Electrochem.* **22** (1992) 1-7.

[173] M. Uchida, Y. Aoyama, N. Eda, A. Ohta, *Journal of The Electrochemical Society* **142** (1995) 4143-4149.

[174] M.S. Saha, A.F. Gullá, R.J. Allen, S. Mukerjee, *Electrochim. Acta* **51** (2006) 4680-4692.

[175] J. Wee, K. Lee, S.H. Kim, *J. Power Sources* **165** (2007) 667-677.

[176] C. Coutanceau, A.F. Rakotondrainibé, A. Lima, E. Garnier, S. Pronier, J. Léger, C. Lamy, *J. Appl. Electrochem.* **34** (2004) 61-66.

[177] C.K. Witham, W. Chun, T.I. Valdez, S.R. Narayanan, *Electrochem. Solid State Lett.* **3** (2000) 497-500.

[178] N. Cunningham, E. Irissou, M. Lefèvre, M.-C. Denis, D. Guay, J.-P. Dodelet, *Electrochem. Solid-State Lett.* **6** (2003) A125-A128.

[179] E. Gülzow, T. Kaz, R. Reissner, H. Sander, L. Schilling, M. v.Bradke, *J. Power Sources* **105** (2002) 261-266.

[180] L. Birry, C. Bock, X. Xue, R. McMillan, B. MacDougall, *J. Appl. Electrochem.* **39** (2009) 347-360.

[181] S. Yılmaztürk, T. Gümüşoğlu, G.A. Arı, F. Öksüzömer, H. Deligöz, *J. Power Sources* **201** (2012) 88-94.

[182] S.C. Thomas, X. Ren, S. Gottesfeld, *J. Electrochem. Soc.* **146** (1999) 4354-4359.

[183] C. Wannek, S. Nehr, M. Vahlenkamp, J. Mergel, D. Stolten, *J. Appl. Electrochem.* **40** (2010) 29-38.

[184] M.A. Abdelkareem, T. Tsujiguchi, N. Nakagawa, *J. Power Sources* **195** (2010) 6287-6293.

[185] B. Krishnamurthy, S. Deepalochani, K.S. Dhathathreyan, *Fuel Cells* **8** (2008) 404-409.

[186] J. Kim, H.Y. Ha, I. Oh, S. Hong, H.N. Kim, H. Lee, *Electrochim. Acta* **50** (2004) 801-806.

[187] H. Dohle, H. Schmitz, T. Bewer, J. Mergel, D. Stolten, *J. Power Sources* **106** (2002) 313-322.

[188] X. Zhao, X. Fan, S. Wang, S. Yang, B. Yi, Q. Xin, G. Sun, *Int. J. Hydrogen Energy* **30** (2005) 1003-1010.

[189] J. Lee, U. Paik, J. Choi, K.K. Kim, S. Yoon, J. Lee, B. Kim, J.M. Kim, M.H. Park, C.W. Yang, K.H. An, Y.H. Lee, *J. Phys. Chem. C* **111** (2007) 2477-2483.

[190] J. Wang, M. Musameh, Y. Lin, *J. Am. Chem. Soc.* **125** (2003) 2408-2409.

[191] C. Boyer, S. Gamburzev, O. Velev, S. Srinivasan, A.J. Appleby, *Electrochim. Acta* **43** (1998) 3703-3709.

[192] X. Xue, C. Bock, L. Birry, B.R. MacDougall, *Fuel Cells (Weinheim, Ger.)* **11** (2011) 286-300.

[193] M.J. O'Connell, P. Boul, L.M. Ericson, C. Huffman, Y. Wang, E. Haroz, C. Kuper, J. Tour, K.D. Ausman, R.E. Smalley, *Chem. Phys. Lett.* **342** (2001) 265-271.

[194] F. Xu, H. Zhang, J. Ilavsky, L. Stanciu, D. Ho, M.J. Justice, H.I. Petrache, J. Xie, *Langmuir* **26** (2010) 19199-19208.

[195] F. Xu, H. Zhang, D. Ho, J. Ilavsky, M. Justics, H. Petrache, L. Stanciu, J. Xie, *ECS Trans.* **41** (2011) 637-645.

[196] H.A. Abaoud, M. Ghouse, K.V. Lovell, G.N. Al-Motairya, *J. New. Mat. Electrochem. Sys.* **6** (2003) 149-155.

[197] H.A. Abaoud, M. Ghouse, K.V. Lovell, G.N. Al-Motairy, *Int. J. Hydrogen Energy* **30** (2005) 385-391.

[198] A.B. Andrade, M.L.M. Bejarano, E.F. Cunha, E. Robalinho, M. Linardi, *J. Fuel Cell Sci. Tech.* **6** (2009) 021305-021305.

[199] D.S. Hwang, C.H. Park, S.C. Yi, Y.M. Lee, *Int. J. Hydrogen Energy* **36** (2011) 9876-9885.

[200] G. Bender, T.A. Zawodzinski, A.P. Saab, *J. Power Sources* **124** (2003) 114-117.

[201] A.D. Taylor, E.Y. Kim, V.P. Humes, J. Kizuka, L.T. Thompson, *J. Power Sources* **171** (2007) 101-106.

[202] S. Towne, V. Viswanathan, J. Holbery, P. Rieke, *J. Power Sources* **171** (2007) 575-584.

[203] R. Benítez, J. Soler, L. Daza, *J. Power Sources* **151** (2005) 108-113.

[204] H.J. Choi, J. Kim, Y. Kwon, J. Han, *J. Power Sources* **195** (2010) 160-164.

[205] H.M. Jhong, F.R. Brushett, P.J.A. Kenis, *Adv. Energy Mater.* **3** (2013) 589-599.

[206] Q. Mao, G. Sun, S. Wang, H. Sun, G. Wang, Y. Gao, A. Ye, Y. Tian, Q. Xin, *Electrochim. Acta* **52** (2007) 6763-6770.

[207] D. You, Y. Lee, H. Cho, J. Kim, C. Pak, G. Lee, K. Park, J. Park, *Int. J. Hydrogen Energy* **36** (2011) 5096-5103.

[208] Y. Chun, C. Kim, D. Peck, D. Shin, *J. Power Sources* **71** (1998) 174-178.

[209] T.V. Reshetenko, H.-T. Kim, U. Krewer, H.-J. Kweon, *Fuel Cells* **7** (2007) 238-245.

[210] M. Yazdanpour, A. Esmaeilifar, S. Rowshanzamir, *Int. J. Hydrogen Energy* **37** (2012) 11290-11298.

[211] A. Lindermeir, G. Rosenthal, U. Kunz, U. Hoffmann, *J. Power Sources* **129** (2004) 180-187.

[212] H. Tang, S. Wang, M. Pan, S.P. Jiang, Y. Ruan, *Electrochim. Acta* **52** (2007) 3714-3718.

[213] T. Frey, M. Linardi, *Electrochim. Acta* **50** (2004) 99-105.

[214] J. Zhang, G. Yin, Z. Wang, Q. Lai, K. Cai, *J. Power Sources* **165** (2007) 73-81.

[215] H. Jung, J.W. Kim, *Int. J. Hydrogen Energy* **37** (2012) 12580-12585.

[216] S. Martemianov, V.A. Raileanu Ilie, C. Coutanceau, *J. Solid State Electrochem.* (2013) 1-9.

[217] C.Y. Chen, C.S. Tsao, *Int. J. Hydrogen Energy* **31** (2006) 391-398.

[218] M. Prasanna, E.A. Cho, T.-H. Lim, I.-H. Oh, *Electrochim. Acta* **53** (2008) 5434-5441.

[219] M.S. Wilson, J.A. Valerio, S. Gottesfeld, *Electrochim. Acta* **40** (1995) 355-363.

[220] P. Liu, G. Yin, E. Wang, J. Zhang, Z. Wang, *J. Appl. Electrochem.* **39** (2009) 859-866.

[221] A. Therdthianwong, P. Manomayidthikarn, S. Therdthianwong, *Energy* **32** (2007) 2401-2411.

[222] U.A. Hasran, S.K. Kamarudin, W.R.W. Daud, B.Y. Majlis, A.B. Mohamad, A.A.H. Kadhum, M.M. Ahmad, *Int. J. Hydrogen Energy* **38** (2013) 9484-9493.

[223] M. Uchida, Y. Aoyama, N. Eda, A. Ohta, *J. Electrochem. Soc.* **142** (1995) 463-468.

[224] S.-J. Shin, J.-K. Lee, H.-Y. Ha, S.-A. Hong, H.-S. Chun, I.-H. Oh, *J. Power Sources* **106** (2002) 146-152.

[225] T. Yang, Y. Yoon, G. Park, W. Lee, C. Kim, *J. Power Sources* **127** (2004) 230-233.

[226] M.C. Tucker, M. Odgaard, P.B. Lund, S. Yde-Andersen, J.O. Thomas, *J. Electrochem. Soc.* **152** (2005) A1844-A1850.

[227] Y. Lee, T.K. Kim, Y.S. Choi, *Fuel Cells* **13** (2013) 173-180.

[228] T.V. Reshetenko, H. Kim, H. Kweon, *J. Power Sources* **171** (2007) 433-440.

[229] P. Liu, G. Yin, C. Du, *Electrochem. Commun.* **10** (2008) 1471-1473.

[230] Z. Wei, S. Wang, B. Yi, J. Liu, L. Chen, W. Zhou, W. Li, Q. Xin, *J. Power Sources* **106** (2002) 364-369.

[231] C.S. Kong, D. Kim, H. Lee, Y. Shul, T. Lee, *J. Power Sources* **108** (2002) 185-191.

[232] J.H. Chun, K.T. Park, D.H. Jo, J.Y. Lee, S.G. Kim, E.S. Lee, J. Jyoung, S.H. Kim, *Int. J. Hydrogen Energy* **35** (2010) 11148-11153.

[233] P. Liu, G. Yin, Y. Shao, *J. Solid State Electrochem.* **14** (2010) 633-636.

[234] G. Liu, Y. Wang, J. Zhang, M. Wang, C. Zhang, X. Wang, *J. Chem. Tech. Biotech.* **88** (2013) 818-822.

[235] S. Mu, C. Xu, Y. Gao, H. Tang, M. Pan, *Int. J. Hydrogen Energy* **35** (2010) 2872-2876.

[236] G. Wang, G. Sun, Q. Wang, S. Wang, J. Guo, Y. Gao, Q. Xin, *J. Power Sources* **180** (2008) 176-180.

[237] S. Park, D. Jung, S. Kim, S. Lim, D. Peck, W.H. Hong, *Electrochim. Acta* **54** (2009) 3066-3072.

[238] J. Nordlund, A. Roessler, G. Lindbergh, *J. Appl. Electrochem.* **32** (2002) 259-265.

[239] Z. Qi, A. Kaufman, *J. Power Sources* **109** (2002) 227-229.

[240] J. Xie, K.L. More, T.A. Zawodzinski, W.H. Smith, *J. Electrochem. Soc.* **151** (2004) A1841-A1846.

[241] J.D. Morse, A.F. Jankowski, R.T. Graff, J.P. Hayes, *J. Vac. Sci. Technol. , A* **18** (2000) 2003-2005.

[242] J.P. Meyers, H.L. Maynard, *J. Power Sources* **109** (2002) 76-88.

[243] S.C. Kelley, G.A. Deluga, W.H. Smyrl, *AIChE J.* **48** (2002) 1071-1082.

[244] M. Müller, C. Müller, F. Gromball, M. Wölfle, W. Menz, *Microsyst. Tech.* **9** (2003) 159-162.

[245] G.Q. Lu, C.Y. Wang, *J. Power Sources* **144** (2005) 141-145.

[246] G. Scotti, P. Kanninen, T. Kallio, S. Franssila, *J. Microelectromech. Syst.* **23** (2014) 372-379.

[247] S.H. Chan, N. Nguyen, Z. Xia, Z.W. Wu, *J. Micromech. Microeng.* **15** (2005) 231-236.

[248] C. Weinmueller, G. Tautschnig, N. Hotz, D. Poulikakos, *J. Power Sources* **195** (2010) 3849-3857.

[249] L. Sainiemi, V. Jokinen, A. Shah, M. Shpak, S. Aura, P. Suvanto, S. Franssila, *Adv. Mater.* **23** (2011) 122-126.

[250] G. Scotti, D. Trusheim, P. Kanninen, D. Naumenko, M. Schulz-Ruhtenberg, V. Snitka, T. Kallio, S. Franssila, *J. Micromech. Microeng.* **23** (2013) 055021.

[251] J. Cao, Z. Zou, Q. Huang, T. Yuan, Z. Li, B. Xia, H. Yang, *J. Power Sources* **185** (2008) 433-438.

[252] A. Kamitani, S. Morishita, H. Kotaki, S. Arscott, *J. Power Sources* **187** (2009) 148-155.

[253] L. Zhong, X. Wang, Y. Jiang, Q. Zhang, X. Qiu, Y. Zhou, L. Liu, *Sens. Actuators, A* **143** (2008) 70-76.

[254] S. Aravamudhan, A.R.A. Rahman, S. Bhansali, *Sens. Actuators, A* **123–124** (2005) 497-504.

[255] Z. Xiao, G. Yan, C. Feng, P.C.H. Chan, I. Hsing, *J. Micromech. Microeng.* **16** (2006) 2014-2020.

[256] J. Yeom, G.Z. Mozsgai, B.R. Flachsbart, E.R. Choban, A. Asthana, M.A. Shannon, P.J.A. Kenis, *Sens. Actuators, B* **107** (2005) 882-891.

[257] N. Kuriyama, T. Kubota, D. Okamura, T. Suzuki, J. Sasahara, *Sens. Actuators, A* **145–146** (2008) 354-362.

[258] F. Zhang, S.G. Advani, A.K. Prasad, *J. Power Sources* **176** (2008) 293-298.

[259] H. Tang, A. Santamaria, J.W. Park, C. Lee, W. Hwang, *J. Power Sources* **196** (2011) 9373-9381.

[260] E.R. Choban, L.J. Markoski, A. Wieckowski, P.J.A. Kenis, *J. Power Sources* **128** (2004) 54-60.

Direct methanol fuel cell (DMFC) produces electricity from methanol without combustion and offers instantaneous recharging by methanol insertion. Therefore, it is a promising candidate for the powering of portable devices. Two obstacles for its commercialization are the high cost and poor performance of catalysts and miniaturization of the components. In this thesis, alternative catalysts for methanol electro-oxidation and oxygen reduction are studied in the fuel cell. It is shown that catalyst layers formed by different types of carbon structures can have widely different porosity affecting the mass transport and the performance of the fuel cell. Low cost carbon-based material is shown to have better performance than expensive platinum. Also, the use of a silicon microstructure (nanograss) is studied as a diffusion layer and electrical contact enhancer in miniaturized fuel cells, which are then used as a material saving platform for catalyst performance testing.

Aalto-DD 76/2014

ISBN 978-952-60-5702-6
ISBN 978-952-60-5703-3 (pdf)
ISSN-L 1799-4934
ISSN 1799-4934
ISSN 1799-4942 (pdf)

Aalto University
School of Chemical Technology
Department of Chemistry
www.aalto.fi